Journal of Computational Neuroscience 3, 51–72 (1996)


# Coding of Odor Intensity in a Steady-State Deterministic Model of an Olfactory Receptor Neuron

JEAN-PIERRE ROSPARS*
*Laboratoire de Biométrie, Institut National de la Recherche Agronomique, 78026 Versailles Cedex, France*
rospars@bmve01.versailles.inra.fr

PETR LÁNSKÝ
*Institute of Physiology and Center for Theoretical Study, Academy of Sciences of the Czech Republic, 142 20 Prague 4, Czech Republic*
lansky@sun1.biomed.cas.cz

HENRY C. TUCKWELL
*School of Mathematical Sciences, Institute for Advanced Studies, Australian National University, Canberra, ACT 0200, Australia; Laboratoire de Biométrie, Institut National de la Recherche Agronomique, 78026 Versailles Cedex, France*
henry@orac.anu.edu.au

ARTHUR VERMEULEN
*Laboratoire de Biométrie, Institut National de la Recherche Agronomique, 78026 Versailles Cedex, France; Laboratoire de Traitement d'Images et Reconnaissance de Formes, Institut National Polytechnique, 38031 Grenoble Cedex, France*
vermeule@bmve01.versailles.inra.fr

*Received April 6, 1995; Revised September 11, 1995; Accepted September 15, 1995*

Action Editor: G. Laurent

**Abstract.** The coding of odor intensity by an olfactory receptor neuron model was studied under steady-state stimulation. Our model neuron is an elongated cylinder consisting of the following three components: a sensory dendritic region bearing odorant receptors, a passive region consisting of proximal dendrite and cell body, and an axon. First, analytical solutions are given for the three main physiological responses: (1) odorant-dependent conductance change at the sensory dendrite based on the Michaelis-Menten model, (2) generation and spreading of the receptor potential based on a new solution of the cable equation, and (3) firing frequency based on a Lapicque model. Second, the magnitudes of these responses are analyzed as a function of odorant concentration. Their dependence on chemical, electrical, and geometrical parameters is examined. The only evident gain in magnitude results from the activation-to-conductance conversion. An optimal encoder neuron is presented that suggests that increasing the length of the sensory dendrite beyond about 0.3 space constant does not increase the magnitude of

*To whom correspondence should be addressed.

the receptor potential. Third, the sensivities of the responses are examined as functions of (1) the concentration at half-maximum response, (2) the lower and upper concentrations actually discriminated, and (3) the width of the dynamic range. The overall gain in sensitivity results entirely from the conductance-to-voltage conversion. The maximum conductance at the sensory dendrite appears to be the main tuning constant of the neuron because it determines the shift toward low concentrations and the increase in dynamic range. The dynamic range of the model cannot exceed 5.7 log units, for a sensitivity increase at low odor concentration is compensated by a sensitivity decrease at high odor concentration.

**Keywords:** sensory coding, cable equation, single neuron modeling

## 1. Introduction

Although much progress has been made in recent years in understanding the physiology of olfactory receptor neurons (e.g., Breer et al., 1990; Zufall et al., 1991; Boekhoff et al., 1993; Menini et al., 1995; reviews of Breer, 1994; Firestein, 1992; Kaissling and Boekhoff, 1993; Shepherd, 1994; Shirsat and Siddiqi, 1993; Stengl et al., 1992), the manner in which the intensity of stimulation is coded remains incompletely understood. The stimulus intensity is measured by the concentration of the stimulating odorant (in the case where it is a pure chemical) whereas the magnitude of the response is usually measured by the frequency of action potentials. This concentration-to-frequency conversion is a basic and well-defined property of olfactory sensory neurons, for which a number of experimentally measured dose-response relationships are available in insects (e.g., Kaissling and Priesner, 1970; Kaissling, 1971; Vareschi, 1971; Selzer, 1984; Kaissling, 1987) as well as vertebrates (e.g., O'Connel and Mozell, 1969; Getchell and Shepherd, 1978; Duchamp-Viret et al., 1989). The biological significance of this problem led us to develop a model of the olfactory receptor neuron.

Several difficulties arise in the development of such a model. A first problem is the paucity of detailed and quantitative information. In the case of olfactory receptor neurons, data are lacking on the second-messenger transduction process and the various ionic conductances involved in the generation of transmembrane potentials. However, such detailed data are probably not needed to account for the main physiological properties of olfactory receptor neurons, as established in classical extracellular recordings, which we consider to be our primary goal. A second problem is the lack of complete solutions to the equations that describe the basic chemical and electrical phenomena under study. Analytical solutions provide irreplaceable references to interpret the numerical solutions that are the only ones presently attainable for more realistic models. For this reason, we subordinated model complexity and realism to mathematical tractability, which lead us to the following choices. One, the complete Hodgkin-Huxley equations for describing the action potential were not considered because their analytical solutions are not available (for their application to an extended neuron, see Rovinsky and Menzinger, 1993); we studied only the time of occurrence (frequency) of the action potentials. Two, only the steady-state behavior of the neuron (constant stimulation) was studied. Three, we did not include stochastic aspects, considered in previous studies (Lánský and Rospars, 1993, 1995; Rospars and Lánský, 1993; Rospars et al., 1994) because the stochastic features play a prominent role when the neuron is stimulated at very low intensities. In these conditions, the deterministic assumptions are not valid. Moreover, the complete solution of the equations that describe the stochastic behavior is presently known only for one-point and two-point model neurons, which are inadequate for our present goal. Four, a receptor neuron with only one type of receptor proteins was studied (such as in the insect sex-pheromone neuroreceptor for example). Five, the variations in diameter of the dendrite, cell body and axon were not taken into account. The dendrite of pheromone receptor neurons of moths is quite close to a long cylinder (Keil, 1984).

The first aim of this paper was to develop, given these assumptions, a model describing the main response variables (that is, conductance change, receptor potential, and firing frequency), and specifying their relationships and their dependence on the biophysical characteristics of the neuron. The cylindrical cable model considered here, which is intermediate between a dimensionless point and complex passive trees (Segev, 1992), is the simplest case permitting one to take into account the spatial extent of the neuron (for a multicompartmental model of the olfactory neuron see

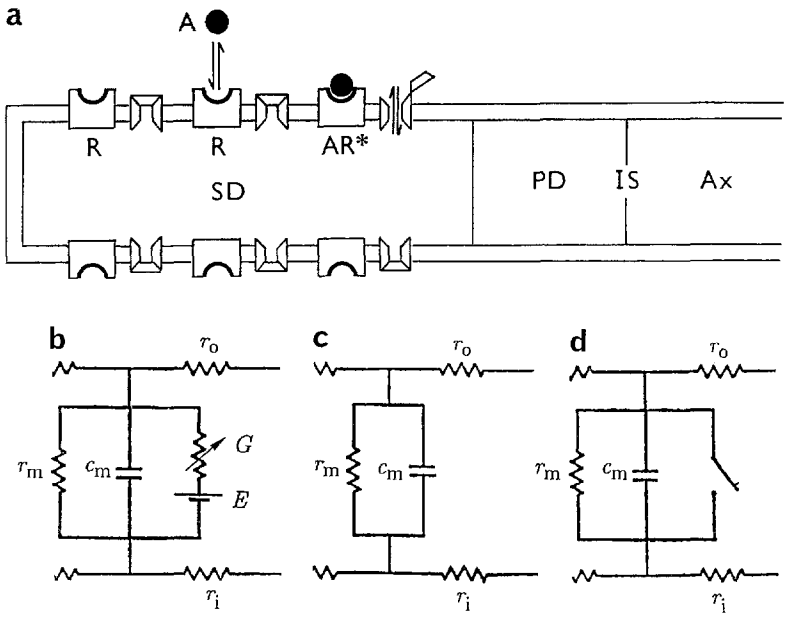


*Figure 1.* (a) Schematic representation of model receptor neuron and equivalent circuits of its three main modules, (b) sensory dendrite SD, (c) passive dendrite PD, and (d) axon initial segment IS. Odorant molecules $A$ bind to receptor proteins $R$ on SD and change their conformation (activated receptors $AR^*$), which ultimately triggers the opening of ion channels. This conductance change $G$, see (b), generates a receptor potential that spreads to IS where action potential are fired and propagated along axon (Ax).

Pongracz et al., 1991). However, none of the known solutions of the cable equation (Rall, 1977; Tuckwell, 1988) describe realistically the stimulation of a sensory neuron. To our knowledge, the solution presented here for an extended, uniform, and steady-state stimulation of the dendrite is original. It describes a realistic case that is useful for describing actual experiments.

Our second aim was to analyze the coding properties of this model. A sensory neuron offers an interesting example for studying neuronal coding in detail because reasonable assumptions can be made on its physiological functions and on how it might code information to fulfill these functions. Coding of the intensity of stimulation is probably the simplest of these tasks. We have analyzed and compared the coding properties of the main neuron responses from transduction to firing using four basic quantities: the concentration at half-maximum response, the lower and upper concentrations actually discriminated, and the width of the dynamic range. These quantities were formalized and their significance discussed with a view to distinguishing the features that directly control the computing performance of neurons from those that result merely from "hardware" constraints. This is a basic issue in theoretical neurobiology that might benefit from the special case studied here.

## 2. The Model

The olfactory neuroreceptor is viewed as a cylinder divided into four regions (Lánský et al., 1994; Fig. 1a). (1) The *sensory component of the dendrite* bears receptor sites; it corresponds mainly to the dendritic cilia of the vertebrate and the outer dendrite of insect neuroreceptors. When activated by odorant molecules, the receptor sites activate a second-messenger system that ultimately opens ionic channels (Section 2.1). This conductance change in turn gives rise to the receptor potential as analyzed in Section 2.2. (2) The *passive region of the dendrite* is assumed to possess no transduction mechanisms and to be a mere cable that passively responds to the receptor potential (also described in Section 2.2). It corresponds to the inner dendrite and cell body membrane. (3) At the *initial segment* of the axon, the receptor potential is converted into a train of action potentials (Section 2.3). (4) The *axon* itself terminates in the brain and is extremely long with respect to the other regions.

### 2.1. *Model of Transduction*

Consider a cylindrical segment of sensory dendrite of unit length with $[R_T]$ receptor sites $R$ of the same type

on its surface and odor-dependent ion channels set in it. This membrane is stimulated by an odor composed of only one molecular type $A$ whose concentration close to the membrane is $[A]$. Since only a thin space in the vicinity of the membrane is relevant for the binding process, $[A]$ can be expressed in moles per unit area ($M$ cm$^{-2}$). The concentration $[R]$ of the receptor molecules is expressed in the same unit. The model of transduction presented here is based on Kaissling's approach (Kaissling, 1969, 1971).

***2.1.1. Number of Activated Receptor Sites.*** Following the initial binding of the odorant molecule to the site and depending on the force of binding, the receptor is "activated", which can be pictured as a change of conformation of the receptor protein. The reactions involved can be written

$$A + R \underset{k_{-1}}{\overset{k_1}{\rightleftarrows}} AR \underset{k_{-2}}{\overset{k_2}{\rightleftarrows}} AR^*, \tag{1}$$

where $k_1$, $k_{-1}$, $k_2$ and $k_{-2}$ denote velocity constants. Then, it can be shown (Ennis, 1991; Getz and Akers, 1995; Malaka et al., 1995; see Appendix A) that

$$[AR^*] = \frac{\dfrac{[R_T]}{K_2 + 1}}{1 + \dfrac{K_1 K_2}{K_2 + 1}\dfrac{1}{[A]}}. \tag{2}$$

Equation (2) depends on the ratio of the velocity constants, the dissociation $K_1 = k_{-1}/k_1$ and deactivation $K_2 = k_{-2}/k_2$ equilibrium constants which have dimension $M$ cm$^{-2}$. It follows that $[A]$ is the only parameter that can be easily changed by the experimenter. In practice $[A]$ has an upper bound, denoted by $[A]_M$, which occurs when air is saturated with $A$, corresponding to the vapor pressure in the actual conditions of temperature and pressure. Although $[A]$ cannot become infinite, we will consider an odorant for which $[A]_M$ is very large with respect to $K_1K_2/(K_2 + 1)$. The graph of (2) as a function of $[A]$ is a branch of hyperbola (for this reason we call such functions "hyperbolic"). The number of activated receptors is zero at $[A] = 0$ and it approaches $[R_T]/(K_2 + 1)$ independent of $K_1$ when $[A] \to \infty$.

***2.1.2. Relation Between Receptor Activation and Conductance Change.*** We assume that the number $n$ of odorant-dependent channels that are opened on the membrane patch at steady state is linearly proportional to the number $[AR^*]$ of activated receptor sites, so that $n = \Gamma[AR^*]$, where $\Gamma$ is the number of channels opened by activation of one receptor molecule. If only a single type of channels is opened, the odorant-dependent conductance in the patch is $G = \gamma n$, where $\gamma$ is the channel conductance. For reasons explained in the next section, we introduce a dimensionless form $g = r_m G$ of conductance $G$ using the resting conductance $r_m^{-1}$ of the membrane patch as unit of conductance,

$$g = r_m \gamma \Gamma [AR^*]. \tag{3}$$

Then putting (2) in (3) we can write, for any $[A]$,

$$g = \frac{g_M}{1 + \dfrac{[A]_{g/2}}{[A]}}, \tag{4}$$

introducing

$$\theta = r_m \gamma \Gamma [R_T] \tag{5}$$

as the conductance when all receptor sites are activated,

$$g_M = \frac{\theta}{K_2 + 1} \tag{6}$$

as the conductance when $[A] \to \infty$, and

$$[A]_{g/2} = \frac{K_1 K_2}{K_2 + 1} \tag{7}$$

as the odorant concentration at which the conductance achieves its half-maximal value $g_M/2$. In the rest of this article we will use $g_M$ and $[A]_{g/2}$ as yardsticks to analyze the receptor potential and the firing frequency. The graph of $g$ versus $[A]$ for (4) is shown and studied in Figs. 2a, 3a, c. Function (4) expressed as a function of $\log[A]$ can be written

$$g = \frac{g_M}{1 + \exp(2.3(\log[A]_{g/2} - \log[A]))}. \tag{8}$$

This is a logistic function whose dependence on $\log[A]$ is sigmoid with an inflection point at $\log[A]_{g/2}$, see Figs. 2b, 3b, d. Equations (3) and (4) implicitly assume that the formation of $[AR^*]$ is the limiting step of the transduction mechanism when $[A]$ increases—that is, $[AR^*]$ reaches its maximum level before any other

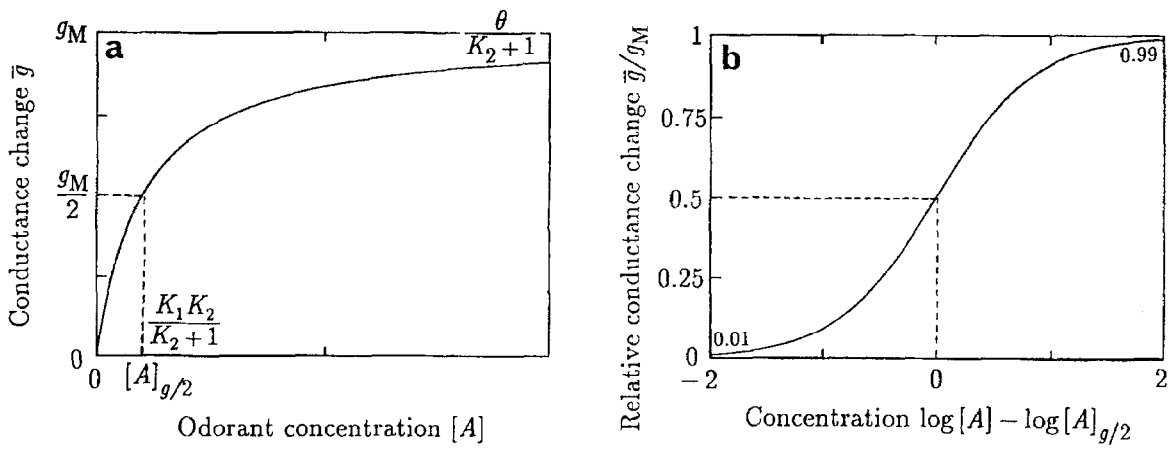


*Figure 2.* Conductance change $\bar{g}$ at any point of the sensory dendrite as a function of odorant concentration $[A]$ (a) and as a function of $\log[A]$, (b). (a) Plot of $\bar{g}$ against $[A]$ is a hyperbolic curve (4) showing maximum value $g_M$ according to (6), and concentration at half-maximum $A_{g/2}$ according to (7) (b) Plot of $\bar{g}/g_M$ against $\log[A]$ is a logistic curve (8) with inflection point at $[A]_{g/2}$; dynamic range for 0.01 according to (9) through (11) is delimited by the sides of the figure. Similar representations apply to number of activated receptor sites $[AR]^*$ (see Eq. (2)) and receptor potential $V_0$ at the distal end of the sensory dendrite (see Eq. (21), (22) and (23)) which are both hyperbolic functions of $[A]$.

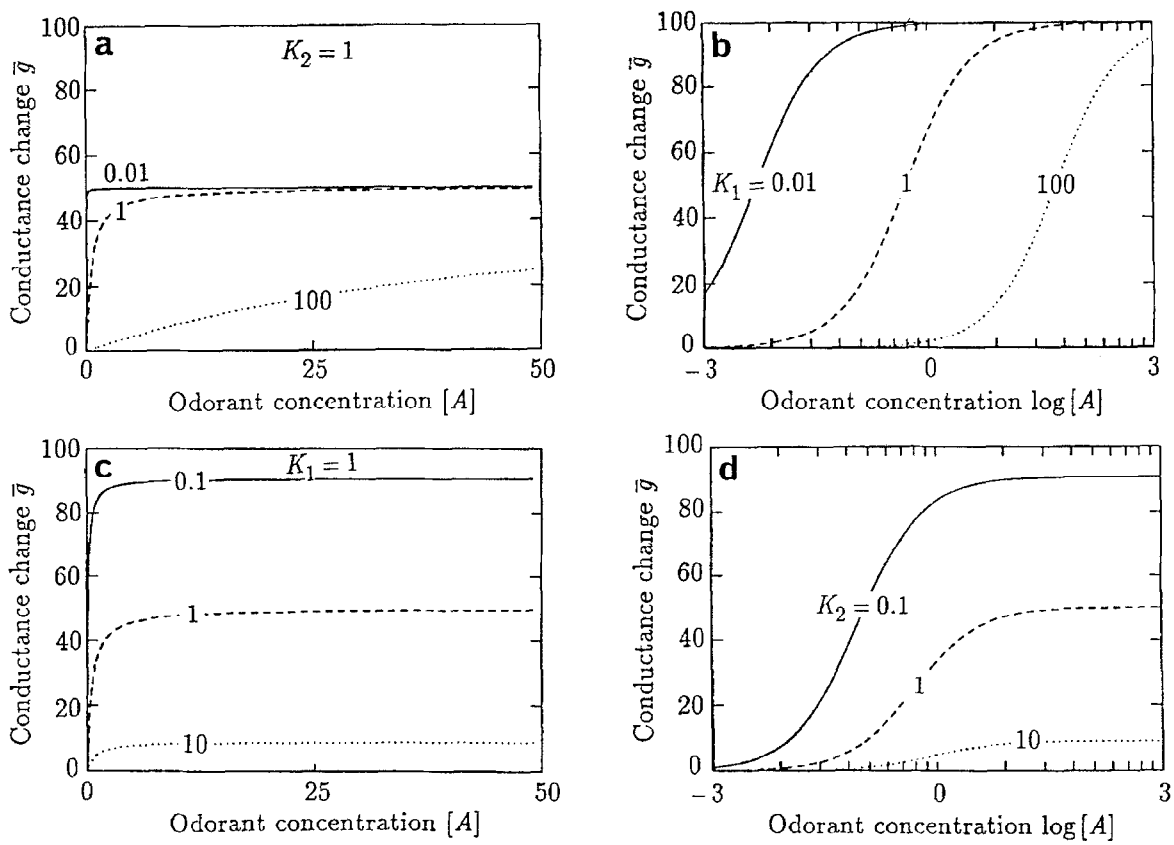


*Figure 3.* Roles of dissociation equilibrium constant $K_1$ and deactivation equilibrium constant $K_2$ on conductance change $\bar{g}$ at the sensory dendrite as a function of odorant concentration $[A]$ (a, c) and $\log[A]$ (b, d) according to (3) through (7). (a, b) Role of $K_1 = 0.01$, 1 and 100 for $K_2 = 1$; $K_1$ acts on response sensitivity, shift from left to right of curves, (b) but not on response magnitude. (c, d) Role of $K_2 = 0.1$, 1 and 10 for $K_1 = 1$; $K_2$ acts on both magnitude and sensivity of response. Parameter $\theta = 100$, conductance that would result from activation of all receptor sites. A similar representation applies to number of activated receptor sites replacing $\theta$ by total number $[R_T]$ of receptor sites.

reaction involved in the activation-to-conductance conversion. Also, as before, we consider here that the maximum value of $g_M$ results from saturation of receptor sites not saturation due to maximum odor concentration $[A]_M$. This caveat holds for all further results based on the assumption $[A] \to \infty$.

*Coding Properties of Conductance Change.* A physiologically significant feature of (4) is to define a specific dynamic range for odorant concentration. Defining the lower bound (threshold) as the concentration $[A]_{gt}$ for which the ratio $g/g_M$ is equal to some arbitrary small value $\epsilon$, such as $\epsilon = 0.01$, and the upper bound (saturation) as the concentration $[A]_{gs}$ for which $g/g_M = 1 - \epsilon$, e.g., 0.99, it can be shown by manipulating (4) that

$$[A]_{gt} = \frac{\epsilon}{1-\epsilon}[A]_{g/2} \simeq \epsilon[A]_{g/2} \tag{9}$$

$$[A]_{gs} = \frac{1-\epsilon}{\epsilon}[A]_{g/2} \simeq \frac{[A]_{g/2}}{\epsilon}. \tag{10}$$

Consequently, the dynamic range $\Delta_g$ for conductance defined as the logarithm of the ratio $[A]_{gs}/A_{gt}$ is

$$\Delta_g = \log[A]_{gt} - \log[A]_{gs} = 2\log\frac{1-\epsilon}{\epsilon} \simeq -2\log\epsilon. \tag{11}$$

This is a constant independent of all neuron characteristics. For example, if $\epsilon = 0.01$, $\Delta_g$ is about 4 log units.

## 2.2. *Model of Receptor-Potential Generation*

***2.2.1. Dendritic Cable.*** For the sake of simplicity we do not take into account the subdivision of the dendrite into several cilia or the variations in diameters (and shape) between dendrite, cell body, and axon. Axial symmetry of the dendrite is assumed over its whole length, and thus only one space variable, the distance $X$ along the dendrite, is needed. The sensory dendrite extends from 0 to $X_1$ and the passive dendrite from $X_1$ to $X_2$ (Fig. 1a). The equivalent circuits for sections of sensory and passive membranes are shown in Figs. 1b and c. The only difference between these circuits is the presence of a variable conductance in the sensory membrane.

The spatiotemporal distribution of the receptor potential $V(X, T)$ along the dendrite generated by the ion current depends on the conductance $g(X, T)$ in the sensory dendrite, which now is given per unit length ($S$ cm$^{-1}$, not unit area as before; for this reason the notations for variables in both cases should have been distinguished, however the corresponding quantities are numerically equal, so that relations (3) through (11) remain valid). In the passive dendrite, by definition, $g(X, T) = 0$. With the above assumptions, $V(X, T)$ is the solution of the cable equation (see Appendix B). In this paper we will focus attention on time-independent steady-state solutions $V(X)$ obtained with $g(X, T) = g(X)$ and in particular those cases where $g(X)$ is a constant over the whole sensory dendrite. It is advantageous to define potential $V(X)$ as membrane depolarization (that is, the resting potential is taken at 0), and to use the space constant $\lambda = \sqrt{\frac{r_m}{r_i + r_o}}$ (cm) as unit of space where $r_m$ is the membrane resistance ($\Omega$ cm), $r_i$ and $r_o$ are the resistances ($\Omega$ cm$^{-1}$) of internal and external mediums respectively, so that $x = X/\lambda$. With these conventions as shown in Appendix B, $V = V(x)$ is the solution of the dimensionless cable equation

$$-\frac{d^2V}{dx^2} + V = g(x)(E - V), \tag{12}$$

where $E$ is the reversal potential of the permeating ion expressed as a depolarization.

***2.2.2. Receptor Potential for a Dendrite with Uniform Stimulation.*** We suppose that the odorant molecules and receptors with their associated ion channels are uniformly distributed along the sensory region of the dendrite. This gives uniform stimulation for which

$$g(x) = \begin{cases} \bar{g} \text{ for } 0 \le x < x_1 \\ 0 \text{ for } x \ge x_1. \end{cases} \tag{13}$$

The steady-state receptor potential $V$ satisfies the differential Eq. (12) and to solve this equation boundary conditions must be chosen. For a semiinfinite cable, the condition at the extremity of the axon is that $V$ is bounded. The other condition is imposed at 0, for example by considering $V(0) = 0$ (killed end) or $V'(0) = 0$ (sealed end). The latter condition, corresponding to a null longitudinal current, is closer to natural conditions and the only one considered in this paper. Under these conditions it is shown in

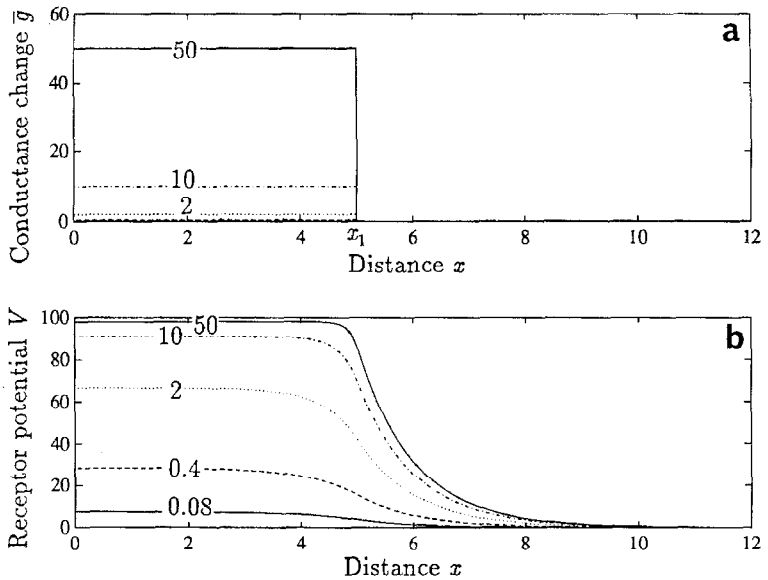


*Figure 4.* Receptor potential along the neuron for different conductance changes at the sensory dendrite. (a) Conductance change as a function of dimensionless distance $x$ according to (13), with proximal end of sensory dendrite at $x_1 = 5$ and $g(x) = \bar{g} = 0.08$ (not shown), 0.4, 2, 10 and 50 over the whole sensory dendrite ($0 < x \leq 5$) and $g(x) = 0$ over passive dendrite and axon ($x > 5$). (b) Corresponding receptor potential $V$ as a function of $x$ according to (14) and (15). Parameter: reversal potential of the odorant-dependent ion current $E = 100$.

Appendix C that the steady-state potential along the cable is

$$V(x) = \begin{cases} \dfrac{E\bar{g}}{1+\bar{g}} \times \left\{1 - \dfrac{\cosh(\sqrt{1+\bar{g}}x)}{\sqrt{1+\bar{g}}\sinh(\sqrt{1+\bar{g}}x_1) + \cosh(\sqrt{1+\bar{g}}x_1)}\right\} & \text{for } 0 \leq x < x_1 \quad (14) \\ \dfrac{E\bar{g}}{1+\bar{g}+\sqrt{1+\bar{g}}\coth(\sqrt{1+\bar{g}}x_1)} \exp(-(x-x_1)) & \text{for } x \geq x_1. \quad (15) \end{cases}$$

The graph of $V(x)$ is shown in Fig. 4 for different values of $\bar{g}$.

***2.2.3. Role of Conductance and Lengths of Sensory and Passive Dendrites.*** The values of the receptor potential at both ends of sensory dendrite (points 0 and $x_1$) and at the initial segment ($x_2$) have a special functional significance. In this subsection we study their dependence on such structural properties of the neuron as the lengths of the sensory and passive dendrites, and on the intensity of stimulation, as reflected in the conductance $\bar{g}$.

*Role of Length of Passive Dendrite for Fixed $\bar{g}$.* The size of the receptor potential at any point beyond $x_1$, and specifically at the axon initial segment $x_2$, given by (15), can be written in the form

$$V(x) = V(x_1)\exp(-(x-x_1)), x \geq x_1, \quad (16)$$

which is completely determined by $V(x_1)$ and the distance from point $x_1$. The input-output properties of the neuron as a whole are thus governed by the length $l_2 = x_2 - x_1$ of the passive dendrite and the value of $V(x_1)$, which depends on $E$, $\bar{g}$ and length $l_1 = x_1$ of the sensory membrane. While the roles of $l_2$ and $E$ are clear, those of $l_1$ and $\bar{g}$ are not immediately apparent

*Role of Length of Sensory Dendrite for Fixed $\bar{g}$ (Fig. 5).* The potential $V(0)$, at $x = 0$, is the maximum depolarization of the sealed-end dendrite. The graphs of $V(0)$ and $V(x_1)$ as a function of $l_1$ for fixed $\bar{g}$ as given by (14) and (15) are shown in Fig. 5. As the length $l_1$ of the sensory dendrite increases both functions rapidly approach asymptotic values $V_0$ and $V_1$

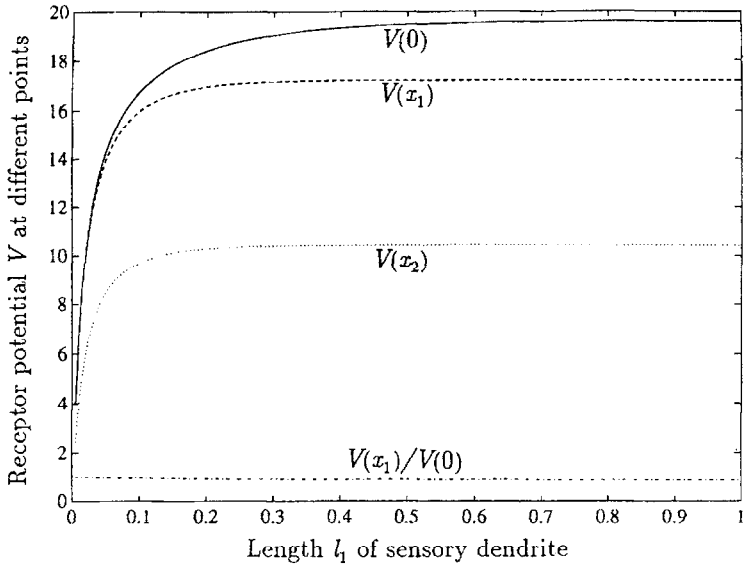


*Figure 5.* Receptor potential at different point as a function of length $l_1 (= x_1)$ of the sensory dendrite. Potential $V(0)$ at distal end of sensory dendrite according to (14), potential $V(x_1)$ at proximal end of sensory endrite and $V(x_2)$ at initial segment according to (15). Ratio $V(x_1)/V(0)$ is constant for a given $\bar{g}$; ratio $V(x_2)/V(x_1)$ is also constant in a given neuron according to (16). For $l_1 > 0.3$ the receptor potential at $x \geq x_1$ is independent of $l_1$. Parameters $E = 20$, $\bar{g} = 20$, $x_2 = x_1 + 0.5$.

defined by

$$V_0 = \lim_{l_1 \to \infty} V(0) \text{ and } V_1 = \lim_{l_1 \to \infty} V(x_1) \qquad (17)$$

In most cases these asymptotic values are nearly attained for $l_1 < 1$ because the quantities $\sqrt{1+\bar{g}}\sinh(\sqrt{1+\bar{g}}x_1) + \cosh(\sqrt{1+\bar{g}}x_1)$ in (14) and $\coth(\sqrt{1+\bar{g}}x_1)$ in (15) tend rapidly to $\infty$ and 1 respectively. The ratio $V_0/V_1$ is $1 + 1/\sqrt{1+\bar{g}}$. Somewhat surprisingly, $V(0)/V(x_1)$ is close to this asymptotic value even for quite small values of $l_1$ (see Fig. 5), which means that the spatial distribution of the receptor potential along the neuron (shown in Fig. 4) is merely shifted to the right when the length of the sensory dendrite increases; this result has obvious functional significance.

*Role of Odorant-Dependent Conductance for Fixed $l_1$ (Fig. 6a, b).* Potentials $V(0)$ and $V(x_1)$ for a given length $l_1$ are increasing functions of $\bar{g}$, which tend to the equilibrium potential $E$, their common asymptotic value. Since the shape of the spatial variation of the receptor potential is practically independent of $l_1$, a study of the dependence of $V(0)$ and $V(x_1)$ on $\bar{g}$ can be performed by considering only $V_0$ and $V_1$ as defined by (17). From (14) the value of $V_0$ is given by

$$V_0 = \frac{E}{1 + 1/\bar{g}} \qquad (18)$$

and from (15) that of $V_1$ by

$$V_1 = \frac{E}{1 + 1/\bar{g} + \sqrt{1+\bar{g}}/\bar{g}} = E\left(1 - \frac{1}{\sqrt{1+\bar{g}}}\right), \qquad (19)$$

which increases more slowly than $V_0$ to their common asymptote as $\bar{g}$ increases. This is illustrated by the conductance at its half-maximum value $E/2$, which is $g_{V_1/2} = 3$, whereas that for $V_0$ is $g_{V_0/2} = 1$ (see Fig. 6a). Let us define $V_2 = \lim_{l_1 \to \infty} V(x_2)$. Then from (16), the asymptotic value of the receptor potential at the initial segment is

$$V_2 = V_1 \exp(-l_2). \qquad (20)$$

Equation (19) thus appears as the major relation describing the conductance-to-voltage conversion of the dendritic part of the neuron.

***2.2.4. Coding Properties of the Receptor Potential.*** The above results show that a study of the receptor

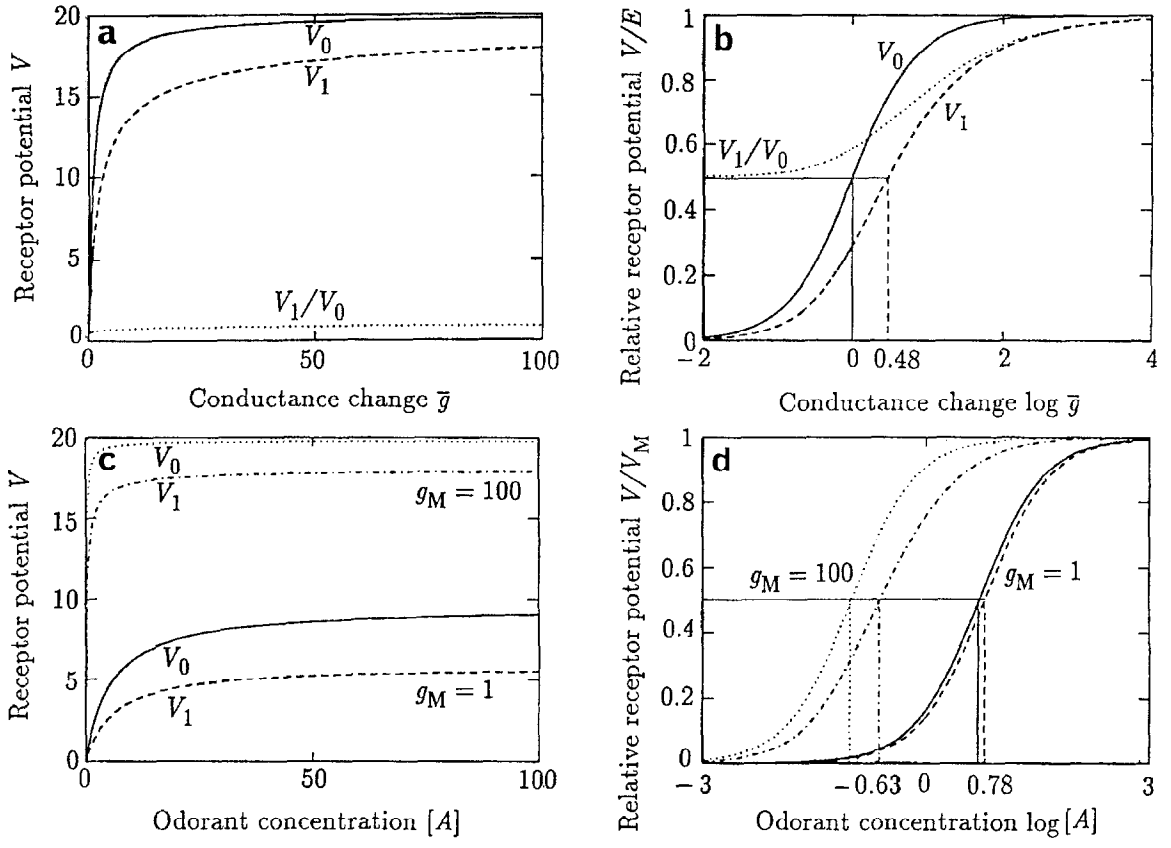


*Figure 6.* Receptor potential at distal end $V_0$ and proximal end $V_1$ of sensory dendrite as a function of conductance $\bar{g}(a, b)$ and odorant concentration $[A](c, d)$. Potential $V_2$ at initial segment (not shown) is a scaled version of $V_1$, see (20). (a) Plot against $\bar{g}$ of $V_0$ according to hyperbolic relation (18) (solid line), $V_1$ according to (19) (dashed line) and their ratio. (b) Plot against log $\bar{g}$ of $V_0/E$ (logistic, solid line), $V_1/E$ (dashed line) and their ratio. Conductances at half-maximum $E/2$ are indicated, with log 3 = 0.48. Dynamic range of $V_1/E$ for $\epsilon = 0.01$ indicated by sides of the figure. (c) Plot against $[A]$ of $V_0$ (hyperbolic) according to (21), (22), and (23) and $V_1$ according to (25), (26), and (27) for $g_M = 1$ (solid and dashed lines) and 100 (dotted and dash-dotted lines). (d) Plot against log$[A]$ of $V_0/V_{0M}$ (logistic) and $V_1/V_{1M}$ for $g_M = 1$ (solid and dashed lines respectively) and $g_M = 100$ (dotted and dash-dotted lines). Concentrations at half-maximum are indicated, from right to left, log$[A] = 0.78, 0.69, -0.63$ and $-1.02$. Parameters $E = 20$ and $[A]_{g/2} = 1$ (in c and d).

potential can be essentially restricted to the asymptotic values $V_0$ and $V_1$. Thus, studying the coding properties of the receptor potential reduces to analyzing how those asymptotic values depend on the stimulus concentration $[A]$ (Fig. 6c, d).

*Maximum Values and Concentrations at Half-Maximum of $V_0$.* Consider first $V_0$, which holds at the distal end of the dendrite and over most of the sensory dendrite. Replacing $\bar{g}$ in (18) by the expression (4) it is found that $V_0$ is again a hyperbolic function of $[A]$

$$V_0 = \frac{V_{0M}}{1 + \dfrac{[A]_{V_0/2}}{[A]}}, \tag{21}$$

where $V_{0M}$ is the maximum value obtained when $[A] \to \infty$ and consequently $\bar{g} \to g_M$ and $[A]_{V_0/2}$ is the concentration at half-maximal $V_0$—that is, recalling (6) and (7),

$$V_{0M} = \frac{E}{1 + 1/g_M} = \frac{E\theta}{\theta + K_2 + 1} \tag{22}$$

$$[A]_{V_0/2} = \frac{1}{1 + g_M}[A]_{g/2} = \frac{K_1 K_2}{\theta + K_2 + 1} \tag{23}$$

The characteristic $V_{0M}$ is itself a hyperbolic function of parameters $r_m$, $\gamma$, $\Gamma$, and $[R_T]$ (see (5)), which reaches its half-maximal value $E/2$ when their product $\theta = K_2 + 1$. The fact that $[A]_{V_0/2} < [A]_{g/2}$ for any set of values of the parameters means that the curve

of $V_0/V_{0M}$ is always above the curve of conductance $g/g_M$ when both are plotted against concentration $[A]$. When plotted against $\log[A]$ the logistic curve for the receptor potential is shifted towards low concentrations relative to the logistic curve for conductance; from (23) the shift is

$$\log[A]_{V_0/2} - \log[A]_{g/2} = -\log(1+g_M). \quad (24)$$

*Maximum Values and Concentrations at Half-Maximal $V_1$.* Consider now the receptor potential at the proximal end of the sensory dendrite from which the potential at any other point beyond $x_1$ can be derived. Replacing $\bar{g}$ in (19) with (4), we obtain $V_1$ as a function of $[A]$ (see Fig. 6c, d)

$$V_1 = E\left(1 - \frac{1}{\sqrt{1+\frac{g_M}{1+\frac{[A]_{g/2}}{[A]}}}}\right), \quad (25)$$

with asymptotic value for $[A] \to \infty$,

$$V_{1M} = E\left(1 - \frac{1}{\sqrt{1+g_M}}\right) = E\left(1 - \sqrt{\frac{K_2+1}{\theta+K_2+1}}\right). \quad (26)$$

Consequently from (20) the asymptotic value of the receptor potential at the trigger zone is $V_{2M} = V_{1M}\exp(-l_2)$. It follows from (26) that the ratio $V_{1M}/E$ becomes greater than $1-\epsilon$ with $\epsilon$ an arbitrarily small value, when $g_M$ is greater than a large value $(\epsilon^{-2}-1)$, e.g., with $\epsilon = 0.1$, $V_{1M}/E = 0.9$ implies $g_M \simeq 100$. For any values of $\theta$ and $K_2$, the inequality $V_{0M} > V_{1M} > V_{2M}$ holds. The odorant concentration $[A]_{V_1/2}$ at half-maximal $V_{1M}$ (which holds also for $V_2$ because $V_1/V_{1M} = V_2/V_{2M}$) is

$$[A]_{V_1/2} = -\frac{4 - \left(1+\frac{1}{\sqrt{1+g_M}}\right)^2}{4-(1+g_M)\left(1+\frac{1}{\sqrt{1+g_M}}\right)^2}[A]_{g/2}. \quad (27)$$

Then, using (23) one finds

$$[A]_{V_1/2} = -\frac{4 - \left(1+\frac{1}{\sqrt{1+g_M}}\right)^2}{\frac{4}{1+g_M} - \left(1+\frac{1}{\sqrt{1+g_M}}\right)^2}[A]_{V_0/2}. \quad (28)$$

These expressions show that $[A]_{V_0/2} < [A]_{V_1/2} < [A]_{g/2}$ for any value of $g_M$—for example, if $g_M = 3$, $[A]_{V_1/2} = 0.35\,[A]_{g/2} = 1.40\,[A]_{V_0/2}$. It follows that $V_1$ and $V_2$ are less "sensitive" to odorant stimulation than $V_0$, whereas the receptor potential at any point is more sensitive than the odorant-dependent conductance change. This "sensitivity" increases with $g_M$, and therefore with $\theta$ and $K_2^{-1}$. The ratios in (27) and (28) remain respectively less than 3 and $3/g_M$, so that the distances at half-maximum between curves plotted against $\log[A]$ are such that

$$\log[A]_{V_1/2} - \log[A]_{V_0/2} \le \log 3 \quad (29)$$

$$\log[A]_{V_1/2} - \log[A]_{g/2} \le \log 3 - \log(1+g_M). \quad (30)$$

*Dynamic Range.* Consider now not the position of the curves along the concentration axis but the range of concentration over which they rise from, say, $\epsilon = 0.01$ to $1-\epsilon = 0.99$ of their maximum value. Because $V_0$ is a hyperbolic function of $[A]$ its threshold concentration $[A]_{V_0t} \simeq \epsilon[A]_{V_0/2}$ and saturating concentration $[A]_{V_0s} \simeq \frac{1}{\epsilon}[A]_{V_0/2}$, where $[A]_{V_0/2}$ is given by (23), have the same forms as those (9) and (10) of the odorant-dependent conductance change. Consequently the dynamic range $\Delta_{V_0}$ is the same as for the conductance, which is given by (11); it is independent of $g_M$. The logistic curves $V_0/V_{0M}$ and $g/g_M$ vs. $\log[A]$ are identical except that the first one is shifted toward low concentration. As a consequence of (27) mentioned above, this shift increases with $g_M$.

The concentrations at threshold $[A]_{V_1t}$ and saturation $[A]_{V_1s}$ for the receptor potential at $x_1$ and $x_2$ derived from (25) are

$$[A]_{V_1t} = -\frac{1-\left(1-\epsilon+\frac{\epsilon}{\sqrt{1+g_M}}\right)^2}{1-(1+g_M)\left(1-\epsilon+\frac{\epsilon}{\sqrt{1+g_M}}\right)^2}[A]_{g/2} \quad (31)$$

$$[A]_{V_1s} = -\frac{1-\left(\epsilon+\frac{1-\epsilon}{\sqrt{1+g_M}}\right)^2}{1-(1+g_M)\left(\epsilon+\frac{1-\epsilon}{\sqrt{1+g_M}}\right)^2}[A]_{g/2}. \quad (32)$$

As shown in Fig. 9, with $\epsilon = 0.01$, whatever $g_M$ the threshold (31) and saturation (32) levels are lower than the corresponding levels for conductance ($\log[A]_{gt} = -2$ and $\log[A]_{gs} = 2$, see (9) and (10)), and $\log[A]_{V_1t}$ decreases faster with $g_M$ than $\log[A]_{V_1s}$ for $10 < g_M < 10^5$. This results in a dynamic range $\Delta_{V_1} = \log[A]_{V_1t} - \log[A]_{V_1s}$ of sigmoid shape as a function of $\log(g_M)$; $\Delta_{V_1}$ is always wider than the 4-decade dynamic range $\Delta_g$ of conductance and tends to 5.7 for large $g_M$.

## 2.3. *Approximate Model of Action-Potential Generation*

***2.3.1. Model of the Initial Segment.*** The axon initial segment that houses the action-potential generator is assumed to be located at $x_2$. It is described by the classical leaky integrator model, which consists of a circuit with a resistor (corresponding to $r_m$), a capacitor (corresponding to $c_m$) and a switch in parallel (Fig. 1d). The switch is assumed to be opened when the membrane potential $V_A$ at the initial segment is below a certain threshold $S_2$ (the subscript 2 indicating that the threshold holds at point $x_2$). When $V_A = S_2$, the switch closes, the capacitor discharges, $V_A$ instantly returns to the resting potential and the switch opens again, which simulates the firing of an action potential. The initial segment has now returned to its initial state and the process can start again. The variable of interest in the model is the time of discharge. To estimate firing frequencies we adopt the following heuristic approach. We assume that the active variable is the current $I(x_2) = V(x_2)/r_m$ flowing through the membrane of the initial segment due to the steady-state receptor potential $V(x_2)$. Starting for example from the resting level (or some other level $v_0 < S_2$) at time $t = 0$ with the switch opened, $I(x_2)$ controls $V_A$. The evolution in time of $V_A$ is a solution of the dimensionless version of the cable equation (48 in Appendix B) with $\partial^2 V/\partial x^2 = 0$ and $I(x_2)$ as the applied current, which is (e.g., Tuckwell, 1988)

$$V_A(t) = V(x_2)(1 - \exp(-t)) + v_0 \exp(-t). \quad (33)$$

Starting from $v_0$, $V_A$ tracks exponentially the constant potential $V(x_2)$.

***2.3.2. Firing Frequency.***

*Voltage-to-Frequency Conversion (Fig. 7a).* The length of interspike intervals and its inverse the firing frequency, can be derived from (33) under the condition that the receptor potential $V(x_2)$ at the initial segment is above the firing threshold $S_2$, $V(x_2) > S_2$, i.e., for a sufficiently high odorant concentration. The firing frequency is

$$f = \left\{ \ln\left( \frac{V(x_2) - v_0}{V(x_2) - S_2} \right) \right\}^{-1} \simeq \frac{V(x_2)}{S_2 - v_0} - \frac{1}{2}. \quad (34)$$

The approximation in (34) holds for $V(x_2) \gg S_2$. However, the difference between $f$ and its approximated value is less than 5% for $V(x_2) > 2S_2$.

*Conductance-to-Frequency Conversion (Fig. 7b).* $V(x_2)$ in (34) is given by (15). The resulting equation can be simplified as follows. First, as mentioned previously, for a sufficiently long sensory dendrite, the asymptotic version $V_2$ given by (20) can be substituted for $V(x_2)$ without significant loss in generality. Second, it is natural to assume that spikes are reset to the resting potential, so $v_0 = 0$. Third, instead of comparing $V_2$ to threshold $S_2$ at initial segment, it is equivalent to compare $V_1$ to threshold $S_1$ defined by

$$S_1 = S_2 \exp(l_2). \quad (35)$$

Then Eq. (34) becomes

$$f = \left\{ \ln\left( \frac{V_1}{V_1 - S_1} \right) \right\}^{-1} \simeq \frac{E}{S_1}\left( 1 - \frac{1}{\sqrt{1 + \bar{g}}} \right) - \frac{1}{2}. \quad (36)$$

*Concentration-to-Frequency Conversion (Fig. 7c).* Replacing conductance $\bar{g}$ by (4), Eq. (36) can be written

$$\begin{aligned} f &\simeq \frac{E}{S_1}\left( 1 - \sqrt{\frac{[A]_{g/2} + [A]}{[A]_{g/2} + (1 + g_M)[A]}} \right) - \frac{1}{2} \\ &= \frac{E}{S_1}\left( 1 - \sqrt{\frac{K_1 K_2 + (1 + K_2)[A]}{K_1 K_2 + (1 + K_2 + \theta)[A]}} \right) - \frac{1}{2}. \end{aligned} \quad (37)$$

***2.3.3. Coding Properties of the Firing Frequency.***

*Maximum Firing Frequency and Concentration at Half-Maximum (Figs. 7d and 8).* According to (34), (35) and (37), the maximum firing frequency of a neuroreceptor when the odorant concentration $[A]$ increases is

$$\begin{aligned} f_M &\simeq \frac{V_{1M}}{S_1} - \frac{1}{2} = \frac{E}{S_1}\left( 1 - \frac{1}{\sqrt{1 + g_M}} \right) - \frac{1}{2} \\ &= \frac{E}{S_1}\left( 1 - \sqrt{\frac{1 + K_2}{1 + K_2 + \theta}} \right) - \frac{1}{2}, \end{aligned} \quad (38)$$

as given for the three major conversion steps—receptor potential, conductance, and transduction respectively. The latter expression shows that $f_M$ increases with the equilibrium potential $E$ and (more slowly) with the conductance $\theta$ and decreases with the deactivation

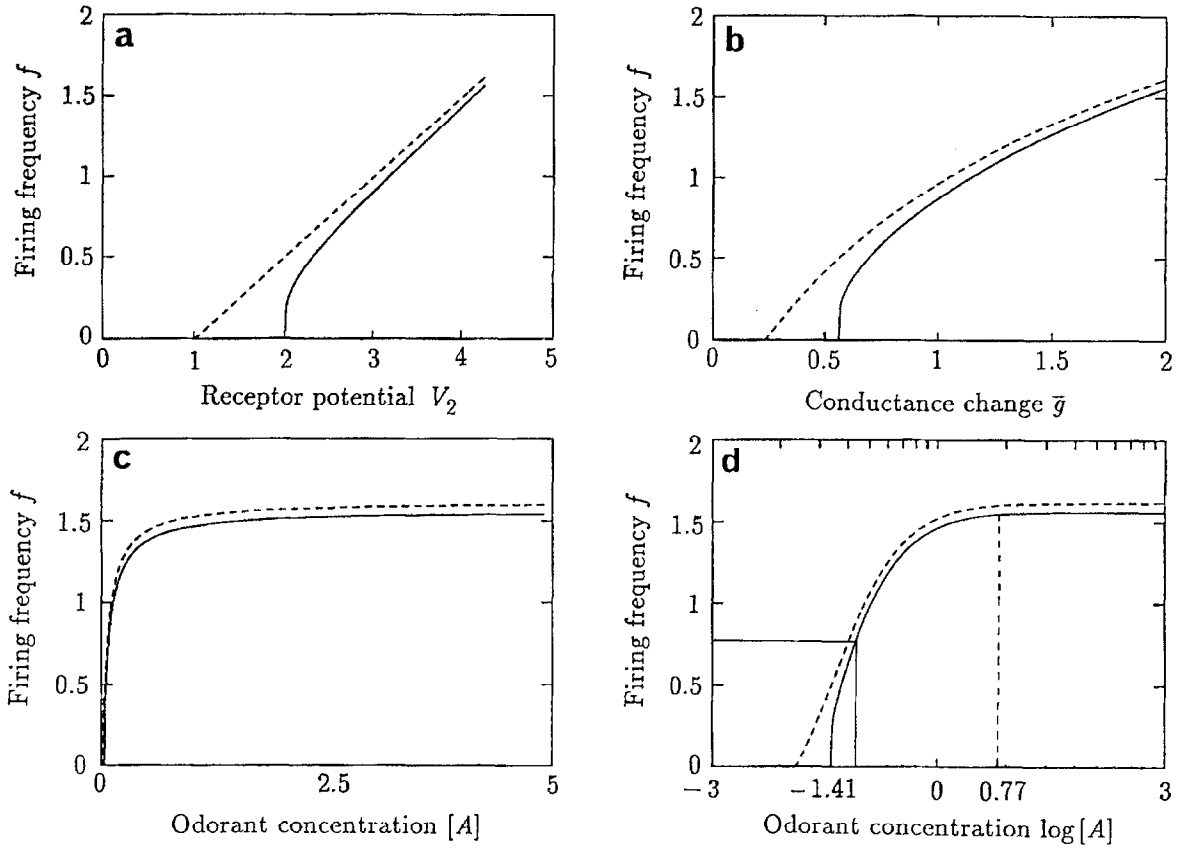


*Figure 7.* Firing frequency $f$ as a function of receptor potential, (a) conductance, (b) and odorant concentration ($c$, $d$). (a) Plot of $f$ against receptor potential $V_2$ at initial segment according to (34). (b) Plot of f against conductance change $\bar{g}$ over sensory dendrite according to (36). (c) Plot of $f$ against odorant concentration $[A]$ according to (37). (d) Plot of $f/f_M$ against $\log[A]$; dynamic range is indicated for $-0.01$. In each plot, frequency is given for exact (full line) and linear approximation (dashed line) as given in (34). Parameters: $E = 20$, $S_2 = 2$, $l_1 = 5$, $\exp(l_2) = 2$ (hence $S_1 = 4$), $g_M = 2$ and $[A]_{g/2} = 0.1$.

constant $K_2$. Of course, the value of $f_M$ in (38) coincides with the experimentally observed maximum firing frequency only if $1/f_M$ is greater than the refractory period.

Using the approximation (36) one derives from (38) the concentration at half-maximal frequency,

$$[A]_{f/2} = -\frac{4 - \left(1 + \frac{1}{\sqrt{1+g_M}} - \frac{S_1}{2E}\right)^2}{4 - (1+g_M)\left(1 + \frac{1}{\sqrt{1+g_M}} - \frac{S_1}{2E}\right)^2}[A]_{g/2}, \tag{39}$$

which is of the same form as (27). From (39) and (23) one can easily derive $[A]_{f/2}$ as a function of $[A]_{V_0/2}$; the expression found is of the same form as (28). Equation (39) shows that the frequency-response curve is shifted toward low concentration with respect to the conductance curve (Fig. 8). For example, with $g_M = 3$, the ratios $[A]_{f/2}/[A]_{g/2}$ and $[A]_{f/2}/[A]_{V_0/2}$ are 0.430 and 1.721 for $S_1/E = 0.1$ and 0.357 and 1.429 for $S_1/E = 0.01$, respectively. The position of curve $f$ with respect to the receptor potential curve $V_1$ is given by the ratio of Eqs. (39) and (27),

$$[A]_{f/2} = \frac{4 - N^2}{4 - M^2} \cdot \frac{4 - M^2(1+g_M)}{4 - N^2(1+g_M)}[A]_{V_1/2}, \tag{40}$$

with $M = 1 + 1/\sqrt{1+g_M}$ and $N = M - S_1/(2E)$. The frequency-response curve is slightly shifted to the right of the receptor potential curve. For example, with $g_M = 3$, the ratio $[A]_{f/2}/[A]_{V_1/2}$ is 1.229 for $S_1/E = 0.1$ and 1.021 for $S_1/E = 0.01$.

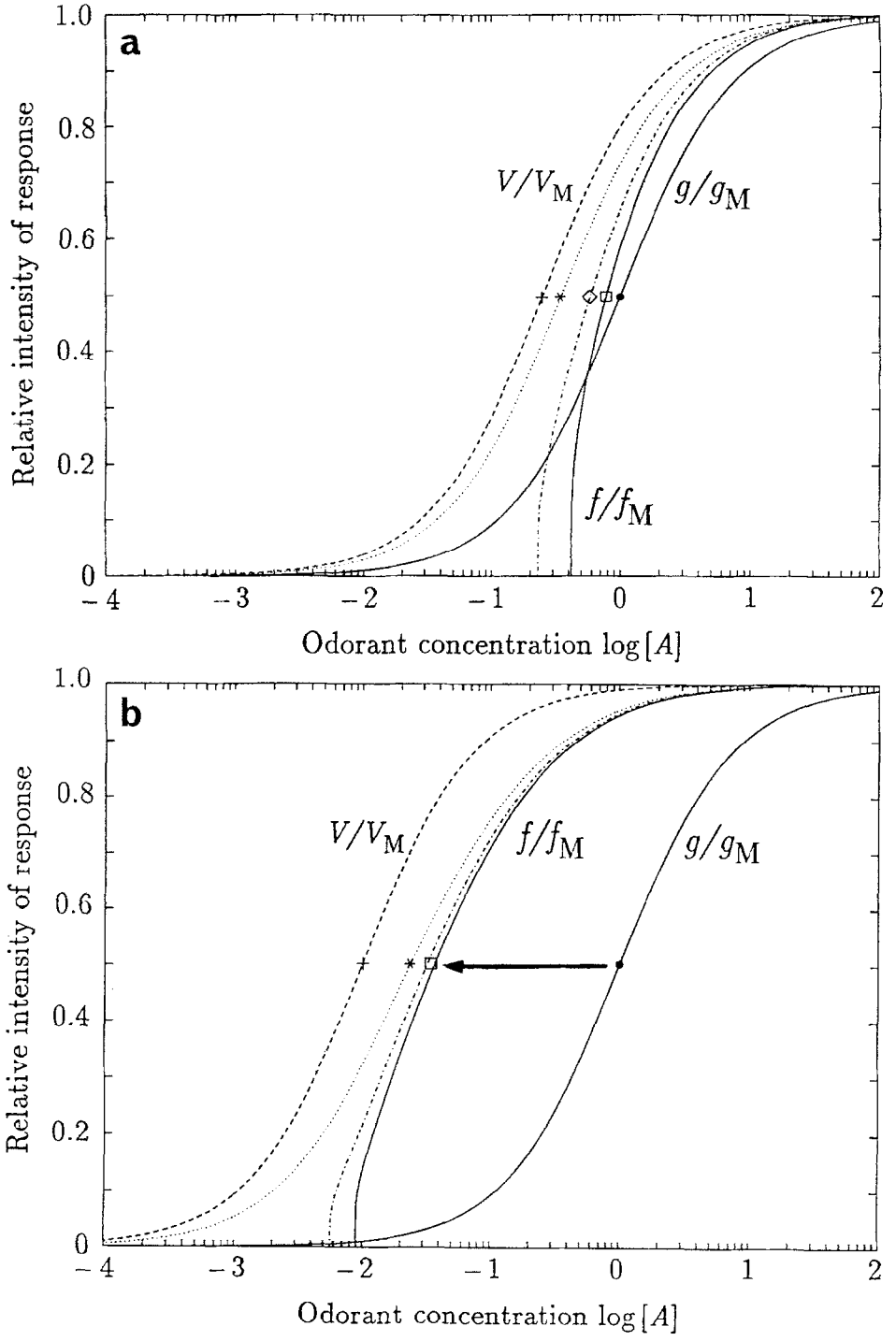


*Figure 8.* Sensitivity of conductance, receptor potential and firing frequency to stimulus intensity. Plot for $g_M = 3$ (a) and $g_M = 100$ (b) of relative magnitude of responses $g/g_M$ (solid line), $V_0/V_{0M}$ (dashed line), $V_1/V_{1M}$ (identical to $V_2/V_{2M}$, dotted line) and $f/f_M$ as a function of log[$A$]. Two $f/f_M$ curves are shown for length of passive dendrite $l_2 = 0$ (dash-dotted line) and $l_2 = 1$ (solid line). Gain in sensitivity in the conductance-to-voltage conversion is displayed as a shift to the left and loss in the voltage-to-frequency conversion as a shift to the right. Concentrations log[$A$] at half-maximum in (a) are 0 ($g$, dot), −0.27 ($f$ for $l_2 = 0$, diamond), −0.46 ($V_1$, star) and −0.60 ($V_0$, cross; in (b) they are 0 ($g$, dot), −1.5 ($f$ for $l_2 = 0$, square), −1.63 ($V_1$, star) and −2.00 ($V_0$, cross). Parameters: $E = 20$, $S_2 = 4$ and $[A]_{g/2} = 1$.

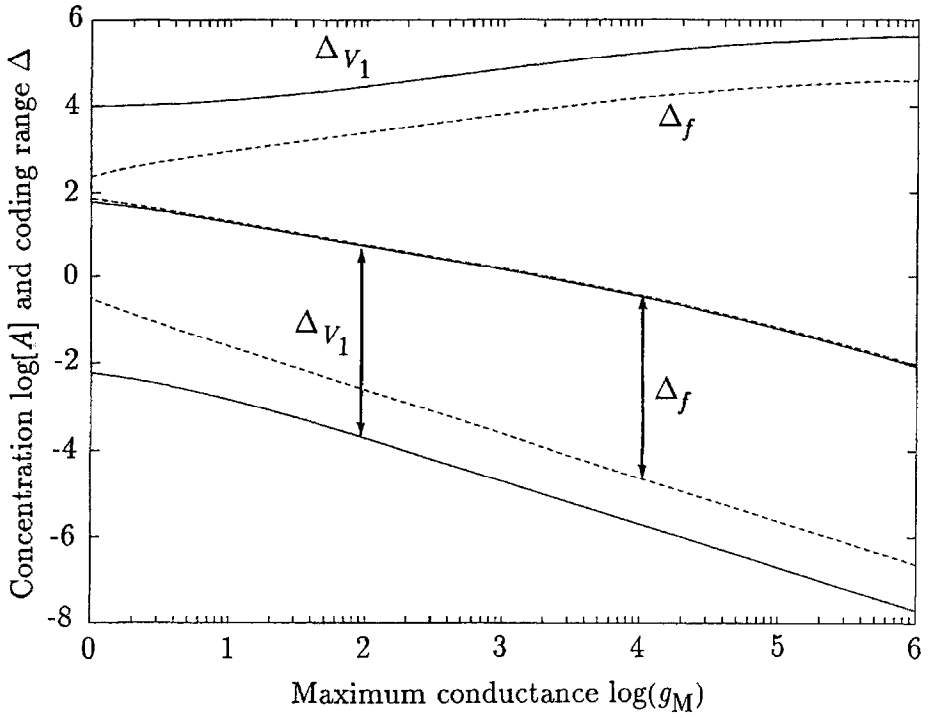


*Figure 9.* Dynamic range and odorant concentrations at threshold and saturation for receptor potential and firing frequency as a function of maximum conductance $g_M$. The curves for receptor potential (solid lines) are given at $x_1$ (or equivalently $x_2$); the concentrations at threshold $\log[A]_{V_{1t}}$ (lower line) and saturation $\log[A]_{V_{1s}}$ (middle line), and the dynamic (coding) range $\Delta_{V_1} = \log[A]_{V_{1t}} - \log[A]_{V_{1s}}$ (indicated by a double arrow; upper line) are computed from (31) and (32). The curves for firing frequency (dashed lines) give the concentrations at threshold $\log[A]_{f_t}$ (lower line) and saturation $\log[A]_{f_s}$ (middle line), and the dynamic range $\Delta_f = \log[A]_{f_s} - \log[A]_{f_t}$ (upper line) based on (41) and (43). For conductance the corresponding values (9) through (11) are independent of $g_M$, $\log[A]_{g_t} = -2$, $\log[A]_{g_s} = 2$ and $\Delta_g = 4$. Parameters: $\epsilon = 0.01$, $S_1/E = 0.1$ and $[A]_{g/2} = 1$.

*Dynamic Range (Figs. 7d and 9).* When the intensity of stimulation increases the neuron model begins to fire when $V_1 = S_1$. Using (19) and (4) the odorant concentration for which this depolarization is reached is

$$[A]_{f_t} = \frac{\frac{S_1}{E}\left(2 - \frac{S_1}{E}\right)}{g_M\left(1 - \frac{S_1}{E}\right)^2 - \frac{S_1}{E}\left(2 - \frac{S_1}{E}\right)}[A]_{g/2}. \quad (41)$$

The concentration $[A]_{f_t}$ decreases linearly with $g_M$ and is always greater than $[A]_{V_{1t}}$ (Fig. 9). The distance between these two curves, which is almost constant for $g_M > 100$ (about 1 log unit for $\epsilon = 0.01$ and $S_1/E = 0.1$), increases with $S_1/E$.

The receptor potential $V_{1f_s}$ for which the firing frequency almost reaches its maximum value $f_s = f_M(1 - \epsilon)$ is such that, according to (38),

$$V_{1f_s} = (1 - \epsilon)V_{1M} + \epsilon\frac{S_1}{2}. \quad (42)$$

The corresponding odorant concentration $[A]_{f_s}$ can be derived from (42) using (4),

$$[A]_{f_s} = -\frac{1 - \left\{\frac{1-\epsilon}{\sqrt{1+g_M}} + \epsilon\left(1 - \frac{S_1}{2E}\right)\right\}^2}{1 - (1 + g_M)\left\{\frac{1-\epsilon}{\sqrt{1+g_M}} + \epsilon\left(1 - \frac{S_1}{2E}\right)\right\}^2}[A]_{g/2}. \quad (43)$$

For $S_1/E$ small enough (0.05 or less) the curves of $[A]_{f_s}$ and $[A]_{V_{1s}}$ as functions of $g_M$ are practically superimposed (Fig. 9). For $g_M > 100$, the dynamic ranges $\Delta_f = \log[A]_{f_s} - \log[A]_{f_t}$ and $\Delta V_1$ as functions of $g_M$ are parallel sigmoid curves separated by about 1 log unit for $\epsilon = 0.01$ and $S_1/E = 0.1$, with $\Delta_f$ tending to 4.67 for large $g_M$, whereas decreasing $S_1/E$ shifts the $\Delta_f$ curve upward, toward the $\Delta V_1$ curve.

## 3. Discussion

A model of an olfactory receptor neuron of cylindrical shape, consisting of a sensory dendrite of length

$l_1$, passive dendrite and cell body of length $l_2$ and semi-infinite axon, was studied under constant stimulation with an odorant at concentration $[A]$ delivered uniformly over the sensory dendrite. This dendritic segment was assumed to bear the same density of receptor proteins $[R_T]$ and ion channels over its whole surface. The activation of each receptor was assumed to produce a uniform increase in conductance $\bar{g}$ at each point of the sensory membrane. The conductance increase, characterized by its maximum values $\theta$ (see (5)), that would result if all receptors were activated, or $g_M$ (see (6)), that would result from very large $[A]$, generated in turn a change in membrane potential which was determined by solving the cable equation. The conversion, above threshold $S_2$, of the receptor potential into a train of action potentials at the axon initial segment was described by a leaky integrator ("RC" circuit), which was assumed to exert no action back on the dendrite.

One of the most thoroughly studied odorant receptor cells is the sex-pheromone neuroreceptor of moths (reviewed in Kaissling, 1986, 1987). We will take this neuron as an example to discuss the assumptions on which the model is based and its properties.

### 3.1. *The Assumptions of the Model in the Context of Experimental Observations*

***3.1.1. Transduction.*** The model describing the transduction process is based on a two-step activation of receptor molecules followed by a linear amplification leading to the opening of the ion channels responsible for the receptor potential. This model is extremely simplified. (1) Although the existence of pheromone receptors on the dendritic membrane is generally accepted, these proteins remain to be identified. The presence of more than one receptor site per receptor protein seems unlikely because it requires only one pheromone molecule to trigger an action potential (Kaissling and Priesner, 1970; Kaissling, 1971, 1990). Consequently, more complex odorant-receptor interactions requiring that several molecules of odorants bind to the receptor (see, e.g., Tateda, 1967) are presently not warranted. (2) Recent investigations (see Stengl et al., 1992, and Kaissling and Boekhoff, 1993, for reviews) have shown that the activated odorant-receptor complexes trigger, via $G$ proteins and phospholipase $C$, a generation on different time scales of several second messengers such as inositol triphosphate, calcium ions and diacylglycerol. A consistent picture of their roles is not yet available. A detailed modeling of these biochemical events (Lamb and Pugh, 1992; Kaissling, 1994) is outside the scope of this paper. Thus, the assumption of a proportionality between the conductance change and the number of activated pheromone-receptor complex remains the most natural one (Kaissling, 1971, 1977, 1987).

***3.1.2. Receptor Potential.*** (1) The cylindrical shape adopted for the dendrite in this study is a reasonable simplification. For example, the outer dendrites of the receptor neurons of *Antheraea polyphemus* are unbranched and the diameter of the thick ones (about 0.5 $\mu$m, Keil, 1984) varies little over most of their length. The construction at the base of the hair, the bulging of the cell soma and the thinner diameter of the axon will have to be taken into account in future development of the model. (2) The receptor potential results from the summation of elementary receptor potentials that can be recorded extracellularly in the absence of pheromone (spontaneous activity) and at very weak stimulation (Kaissling, 1986, 1987). The conductance change underlying the elementary receptor potentials was calculated to be in the range of 30 pS (Kaissling, 1986), which may be interpreted as the opening of a single channel or of several channels of smaller conductance (Kaissling, 1994). (3) The ions carrying the receptor current are not known. Cation channels activated by second messengers with reversal potential around 0 mV were demonstrated, some selective to $K^+$ and others to both $K^+$ and $Na^+$. Their role in the generation of the receptor potential remains to be investigated. No gradient across the membrane is expected for $K^+$ because its concentration in the sensillum lymph that surrounds the sensory dendrite is very high (Kaissling and Thorson, 1980). (4) This suggests that the voltage source for the receptor potential in the moth neuroreceptor might not be the battery $E$ at the sensory dendrite, as assumed in the single neuron model presented here, but, in part, the transepithelial potential $E_t$ created by the neuron's auxiliary cells in the sensillum. No intracellular recordings of the receptor neuron having yet been possible, what is known using extracellular electrodes is the receptor potential modified by the auxiliary cells (sensillar potential, Stengl et al., 1992). These cells separate an outer segment in the sensillum lymph and an inner segment in the hemolymph. An equivalent circuit model of the sensillum has been developed (Kaissling,

1971; Kaissling and Thorson, 1980; de Kramer et al., 1984; de Kramer, 1985) based on this compartimentalization and different space constants for the corresponding cable dendrites. An equation derived by J. Thorson (cited by Kaissling, 1971) applies when the potential $E_t$ between compartments is the only voltage source in the sensillum; it gives the potential at the junction between the segments and thus corresponds to Eq. (15) at $x = x_1$ for a neuron in isolation.

***3.1.3. Action Potentials.*** (1) The generating site of the action potentials is believed to be at the inner dendrite or at the soma region, although the exact location is not known (Kaissling, 1987). Both locations can be easily fitted to the present model. (2) Passive backpropagation of the action potentials along the dendrite has not been considered because the corresponding equations are difficult to solve. It follows that the model is asymmetric, the dendritic compartment influencing the axonal compartment but not vice versa (see discussion in Rospars and Lánský, 1993). However, backpropagation can be incorporated using numerical techniques (Vermeulen et al., 1995) and analytical solutions are now available (Bressloff, 1995) for a simplified action potentials with a downward deflection (reset) but no peak. (3) The spike encoding mechanism used in this paper is based on a leaky integrator and is thus very simplified. This is the only model to our knowledge for which the spike frequency can be derived analytically from a knowledge of the dendritic potential. This basic scheme will be compared later with more realistic models with multiple conductances (see, e.g., Wilson and Bower, 1989; Yamada et al., 1989; Schwaber et al., 1993; Av-Ron, 1994), which have the inconvenience of being solved numerically and of being based on channel properties that are not yet completely known.

Three saturating mechanisms are present in the model: one results from the odorant-receptor interaction, the second from the conductance-to-voltage conversion, and the third from the voltage-to-firing conversion. Other nonlinearities can be present, related for example to odorant transport (Kaissling, 1990; Hahn et al., 1994) and to the second-messenger system. The model assumes merely that the steps studied are the limiting ones. Moreover, the model has been presented in the case where the saturation at a given level is reached before saturation at any previous level (see (38)). The alternative assumptions will be considered when applying the model to experimental data.

### *3.2. Magnitude of Responses*

The analyses carried out have shown that the properties of the model can be conveniently divided into two groups, related to the magnitude and the sensitivity of the neuron physiological responses. This neat subdivision holds only for a deterministic model, i.e., for $[A]$ not too small (the stochastic case that prevails at weak stimulation is briefly considered in the last section). Let us consider first the magnitudes of the various responses studied—that is, (1) conductance, (2) receptor potential, and (3) firing frequency, and their asymptotic values $g_M$, $V_M$ and $f_M$, as $[A]$ increases.

(1) The *odorant-dependent conductance* $\bar{g}$ at any point of the sensory dendrite was found to vary as a hyperbolic function of $[A]$ according to (4) and consequently as a logistic function of $\log[A]$ (Fig. 2). The maximal conductance $g_M$ (6) is proportional to the total conductance $\theta$, independent of the dissociation constant $K_1$ (Fig. 3b) and inversely related to the deactivation constant $K_2$ (Fig. 3d), confirming the previous results of Kaissling (1987). The quantity $g_M$ plays a central role because it determines most of the functional properties of the model as shown in the following discussion. The dependence of $\bar{g}$ on $[A]$ has been determined in voltage-clamp conditions in a vertebrate neuroreceptor (Menini et al., 1995) showing that it is not exactly hyperbolic but is better described by a Hill equation. The origin of this cooperative feature remains to be determined.

(2) The longitudinal profile of the *receptor potential* $V(x)$ is nearly constant over the distal part of the sensory dendrite and begins to fall near its proximal end (see (14) and (15) and Fig. 4b). This profile is translated when the length $l_1$ of the sensory dendrite is changed, provided that $l_1$ is greater than about 0.3 space constants (Fig. 5). Under this condition, an almost complete description of the dependence of the receptor potential on $\bar{g}$ and $[A]$ can be given by specifying $V(x)$ at only two points, the proximal and distal ends of the sensory dendrite. The potential $V_0$ at the distal end corresponds to the solution given by Kaissling

(1987, Fig. 32); it is a hyperbolic function of $\bar{g}$ ((18) and Fig. 6a, b) with asymptotic maximum $E$ and a (different) hyperbolic function of $[A]$ ((21) and Fig. 6c, d), with maximum approaching $E$ when $g_M$ increases. However, the most relevant value of the receptor potential is $V_1$, at the proximal end of the sensory dendrite, because it determines the potential at the spike trigger zone, $V_1 \exp(-l_2)$. Potential $V_1$ is a nonhyperbolic function of $\bar{g}$ (19) reaching more slowly its asymptotic maximum $E$ than $V_0$ (Fig. 6b). Also, unlike $\bar{g}$ and $V_0$, potential $V_1$ is not a hyperbolic function of $[A]$ ((25) and Fig. 6c, d), although it has also a horizontal asymptote at level $V_{1M} < E$. Maximum $V_{1M}$ (26) slowly approaches $E$ when $g_M$ increases. This dependence of $V_1$ on $\log[A]$ is in accordance with the experimental measurements of the sensillar potential, both curves displaying a less steep slope than that expected from a logistic function (see, e.g., Fig. 29 in Kaissling, 1987).

(3) The *firing frequency* $f$, unlike conductance and potential, does not start at the origin but remains zero for all depolarizations of the trigger zone smaller than the firing threshold $S_2$ or, equivalently, for all depolarizations $V_1$ smaller than $S_1 = S_2 \exp(l_2)$. However, $f$ quickly approaches a linear function of $V_1$ (36) with a slope inversely proportional to $S_1$, only limited by the refractory period (Fig. 7a). Consequently, $f$ is a nonhyperbolic function of $[A]$ ((37) and Fig. 7c), whose maximum $f_M$ is proportional to $V_{1M}$ and inversely proportional to $S_1$, and tends to $E/S_1$ for large $g_M$. The voltage-to-frequency conversion step appears to present two negative features. First, due to the passive segment, it codes a signal $V_2$ that is weaker than those ($V_0$ and $V_1$) resulting from the transduction process. Second, the original signal is either not converted below threshold or converted in a highly nonlinear way just above it, so that the model neuron is not an accurate encoder in this range of values of the receptor potential. The properties below and at the vicinity of the threshold being dominated by stochastic properties (see Section 3.4) only the right part of the curve can be meaningfully compared to experimental data. Like the sensillar potential, the curve of the measured frequency versus $\log[A]$ has a slope that is less steep than that of a logistic curve, which is in accordance with the model.

It follows from the results for this model that an optimal encoder neuron for odorant intensity—that is, delivering signals over a wide band (up to $g_M$, $V_M$ and $f_M$)—would have small equilibrium dissociation constant $K_2$, large total conductance $\theta$ (by a combination of high resting membrane resistance $r_m$, large number $[R_T]$ of receptor proteins, large number $\Gamma$ of channels per receptor and high channel conductance $\gamma$), large equilibrium potential $E$, relatively short sensory dendrite ($l_1$ about 0.3 space constant), passive dendrite as short as possible, and very small firing threshold $S$. Of course, the model did not take into account factors that are biologically important and can act in the opposite direction. For example, the sensory dendrite of the pheromone receptor cell is not only a voltage encoder but also a molecular collector. The result of the model that increasing its length above about 30% of the space constant (that is, ca. 100 $\mu$m, Kaissling, 1987) does not increase the receptor potential at the axon initial segment suggests that its long length (up to 300 $\mu$m, Kaissling, 1987) contributes mainly to increase the capture area for pheromone molecules. Consequently, receptors for odors for which molecularcapture is not so critical should not be so long. This is what is observed in moths with the receptor cells adapted to general odorants (such as plant odors) that are not detected at concentrations as low as those for the pheromone signal. The model suggests that the observed dendritic length in pheromone receptor neurons is not primarily explainable in terms of transduction or electrical processes.

### 3.3. *Sensitivity of Responses*

Whatever its magnitude, the more *sensitive* a response is, the less intense the stimulus needs to be to evoke it. To analyze the sensitivity of the responses, based on this definition, their relative magnitudes (that is the ratios $\bar{g}/g_M$, $V/V_M$ and $f/f_M$) were plotted against $\log[A]$, which is the most practical measure of stimulus intensity. Then the curves could be directly compared within the same reference system and the gain (shift to the left, toward low concentrations) and loss (shift to the right) in sensitivity easily determined (Fig. 8). The following analysis is not rigorous for the smallest detectable concentrations discussed in paragraph (2) because, at these low concentrations, the validity of the deterministic model is questionable (see

Section 3.4). Nonetheless these values are useful to know.

(1) The positions of the response curves with respect to each other were first studied using the *concentration at half-maximum response* $\log[A]_{r/2}$, which gives the positions of the responses $r$ along the intensity axis. First, it follows from the assumption that conductance is a linear function of the number of activated receptors that the activation-to-conductance conversion (transduction) has no effect on sensitivity; $\log[A]_{[AR^*]/2}$ and $\log[A]_{g/2}$ are equal, see (2). Second, the conductance-to-voltage conversion increases the sensitivity as evidenced by the fact that the curve for $V_0$ is shifted by $\log(1+g_M)$ to the left of the conductance curve, see (24). This effect is counteracted by the spreading of the voltage over the passive segment; the curves for $V_1$ and $V_2$, which are superimposed, are shifted to the right of $V_0$ by an amount that increases with $g_M$, see (28), which means that the receptor potential at the spike generating segment is slightly less sensitive than that at the distal part of the dendrite. Nonetheless, unlike the transduction step, the conductance-to-voltage conversion shifts the receptor potential at any point along the dendrite toward lower concentrations. Third, the voltage-to-frequency conversion shifts the frequency curve to the right of the receptor potential curve according to (40), but the corresponding loss in sensitivity appears to be small (Fig. 8). On the whole, for $g_M$ large enough, the gain in sensitivity is of the order of $\log(g_M)$. It appears also that the distance $l_2$ of the axon initial segment to the proximal end of the sensory dendrite has a weak effect on the sensitivity of the firing response as shown on Fig. 8 by the close proximity of the frequency curves for $l_2 = 0$ and $l_2 = 1$ space constant. The main conclusion of this analysis is that the gain in magnitude and the gain in sensitivity can be ascribed to two distinct mechanisms—the activation-to-conductance conversion acting on the magnitude of the signal and the conductance-to-voltage conversion on its sensitivity. All other conversion steps are either neutral or entail a cost in terms of gains.

(2) The smallest concentration $\log[A]_{r_t}$ at which the response $r$ can be discriminated from 0 (*sensory threshold*) and the largest $\log[A]_{r_s}$ at which it becomes indistinguishable from 1 (*saturation level*) were formalized and located with respect to $\log[A]_{r/2}$. For all responses, except the lower value of firing frequency, the same criterion was used—that is $r$ rising above baseline by an arbitrary value $\epsilon$ (e.g., 0.01) or reaching $1-\epsilon$ (e.g., 0.99) just below the upper asymptote. For the conductance the lower and upper concentrations are located symmetrically on both sides of $\log[A]_{g/2}$, at $\log[A]_{g/2} \pm \log\epsilon$ (Fig. 2b). This symmetry being a property of the logistic function, holds also for the potential $V_0$ with respect to $\log[A]_{V_0/2}$. For the potential $V_1$ (Fig. 6d), the study of Eqs. (28), (31) and (32) shows that $\log[A]_{V_{1t}}$ and $\log[A]_{V_{1s}}$ become asymmetrical for large $g_M$ with the first half-range from $\log[A]_{V1t}$ to $\log[A]_{V_1/2}$ being shorter than the second half-range. The frequency response curve (Fig. 7d) presents a similar asymmetry as a consequence of relations (39), (41) and (43). When $g_M$ increases the threshold levels of $V_1$ and $f$ remain in a constant ratio and their saturation levels are almost the same (Fig. 9). The almost parallel decrease of these levels with $g_M$ show that diminishing the threshold in this way diminishes also the saturation level. This suggests that different neuron types must encode weak and strong stimuli.

(3) The last characteristics are the *dynamic ranges* of the various responses, $\Delta_r = \log[A]_{rs} - \log[A]_{rt}$. The last two conversion steps can increase the fixed range (4 log units) imposed by the logistic equation describing the early steps of the encoding process. It is significant, as shown in Fig. 9, that the dynamic range for $V_1$, which represents the "useful" receptor potential ultimately converted in a train of action potentials, increases with the maximum conductance change $g_M$ and that the dynamic range for $f$ increases with $g_M$ and decreases with increasing $S_1/E$, which is another fundamental "tuning" constant of the neuron. The maximum dynamic range found in the model for both the receptor potential (at very large $g_M$) and the firing frequency (at very small $S_1/E$) is 5.7 log units. Although the order of magnitude is correct, this is less than the dynamic range of 6 or more log units that have been reported for frequency (e.g., Fig. 29 in Kaissling, 1987).

### 3.4. *Future Developments*

Besides the problems related to neuron variable diameter, spike backpropagation into the dendrite, action-potential generator and cell environment, two major

developments are to be considered—the evolution of the neuron response in time and a stochastic generalization of the model applicable to stimulation at low concentration. Both developments concern physiologically significant features of sex-pheromone receptor cells, for example, because these neurons react at very low concentration and follow fast temporal variations of the stimulus concentration known to occur in pheromone plumes.

The present model describes the neuron at steady state only. It is known that the receptor potential of sex-pheromone receptor neurons reaches this state in a fraction of a second after the onset of stimulation, its half time-to-peak being 300 ms for weak stimulation and 50 ms for strong stimulation (Fig. 29 in Kaissling, 1987). The evolution of the system toward equilibrium was analyzed in a stochastic context by Lánský and Rospars (1993) and is also considered in Tuckwell et al. (1995). With solutions of the complete space- and time-dependent cable equation the model could be extended to stimulation varying in time.

The transduction model studied is only an approximation at very low odorant concentration because enough receptor proteins must be activated in order to apply Eq. (2) (it describes a continuous-state model that holds only for $[AR^*] \gg 0$, which implies that $[R_T]$ and $[A]$ are also very high). A similar remark holds for the conductance change because it is also discrete as evidenced by the existence of elementary receptor potentials (Kaissling, 1994). When only a few occupied receptor sites play a significant role in the neuron behavior (Kaissling and Priesner, 1970; Kaissling, 1971; Lynch and Barry, 1989; Menini et al., 1995; see also Lundström et al., 1993 and Lowe and Gold, 1995) a stochastic generalization of the odorant-receptor interactions must be used.

In previous work (Lánský and Rospars, 1993; Rospars and Lánský, 1993) we described the reactions in (1) by a stochastic birth-and-death process (occupation) and a stochastic transition of fixed probability $p$ (activation). Equation (11) in Lánský and Rospars (1993) for the steady-state mean number of activated receptors is to be compared with (2) above, with $k_1[A]$ and $k_{-1}$ corresponding to the birth-parameter $\lambda$ and death-parameter $\mu$ respectively. It can easily be shown that both equations are equal only if $1/p = K_2$ and $K_2 + 1 \approx K_2$—that is, if the probability $p$ of activation is very low, which implies, knowing the condition (5) for equilibrium, that this model of activation is valid only in the special case $[AR] \gg [AR^*]$. This means that a fully satisfactory stochastic description of the receptor occupation and activation remains to be developed, a notoriously difficult problem (Nicolis and Prigogine, 1977). However stochastic modeling is achieved, it must be realized that stochastic mechanisms have the important property to lower the firing threshold $[A]_{f_1}$ (Yu and Lewis, 1989; Gerstner and van Hemmen, 1992; Segundo et al., 1994; Lánský and Rospars, 1995). So, any satisfactory description of the dynamic range of neurons will have to take this feature into account.

## Appendix A: Number of Activated Receptor Sites

According to the basic equation of chemical kinetics the velocities of the forward $(v_1, v_2)$ and backward $(v_{-1}, v_{-2})$ reactions in (1) are $v_1 = -\frac{d[A]}{dt} = k_1[A][R]$, $v_{-1} = \frac{d[A]}{dt} = k_{-1}[AR]$, $v_2 = -\frac{d[AR]}{dt} = k_2[AR]$, $v_{-2} = \frac{d[AR]}{dt} = k_{-2}[AR^*]$. The equilibrium (steady state) is reached when $v_1 = v_{-1}$ and $v_2 = v_{-2}$. It implies that

$$[A][R] = (k_{-1}/k_1)[AR] \tag{44}$$

and

$$[AR] = (k_{-2}/k_2)[AR^*]. \tag{45}$$

Concentration $[A]$ can be considered constant because the number of molecules $A$ present in the vicinity of the membrane is permanently kept in equilibrium by diffusion from the outer space. Thus, $[A]$ is not significantly decreased by the loss of some $A$ to form $AR$. We do not assume the same property for receptor sites, so that the $[R_T]$ receptors can be in three states:

$$[R_T] = [R] + [AR] + [AR^*]. \tag{46}$$

Putting (46) in (44) and (45), we get $[AR^*]$ as a function of $[A]$; see (2).

## Appendix B: Cable Equation for a Sensory Dendrite

We are interested in the spatiotemporal distribution $V = V(X, T)$ of the receptor potential generated by an ion current that depends on the conductance $G(X, T)$ in the sensory dendrite. When $V$ is defined as membrane depolarization—that is, $V = \tilde{V} - V_r$, where $\tilde{V}$ is the actual membrane potential and $V_r$ is the resting

potential—$V$ is the solution of the cable equation (Rall, 1989; Tuckwell, 1988, Ch. 4):

$$-\frac{r_m}{r_i+r_o}\frac{\partial^2 V}{\partial X^2}+r_m c_m\frac{\partial V}{\partial T}+V=\frac{r_m}{r_i+r_o}(r_i I_i-r_o I_o), \tag{47}$$

where $r_m$ is the membrane resistance ($\Omega$cm), $r_i$, $r_o$ are the resistances ($\Omega$ cm$^{-1}$) of internal and external mediums respectively, $c_m$ the membrane capacitance ($F$ cm$^{-1}$), $I_i = I_i(X, T)$ and $I_o = I_o(X, T)$ are the applied current densities ($A$ cm$^{-1}$) in the internal and external mediums. In the case of a passive cable (see Rall, 1989), there is no applied current, $I_i = I_o = 0$, except if the experimenter injects a current with an electrode. In the case of a sensory dendrite, assuming that an ionic current $I$ flows inwardly through the open odorant-dependent channels and adopting the convention that the inward currents are positive, we have $I_i = I$ and $I_o = -I$, and consequently the right hand side of (47) reduces to $r_m I$:

$$-\frac{r_m}{r_i+r_o}\frac{\partial^2 V}{\partial X^2}+r_m c_m\frac{\partial V}{\partial T}+V=r_m I(X,T). \tag{48}$$

Now, the ionic current $I$ is $I(X, T) = G(X, T)\times(E - V)$, where depolarization $E = \tilde{E} - V_r$ corresponds to the reversal potential $\tilde{E}$ of the permeating ion. Using the space constant $\lambda = \sqrt{\frac{r_m}{r_i+r_o}}$ as unit of space, $x = X/\lambda$, the time constant $\tau = r_m c_m$ as unit of time, $t = T/\tau$, and the membrane conductance at rest $r_m^{-1}$ as unit of conductance, i.e., $g(x, t) = r_m G(x, t)$, Eq. (48) becomes the dimensionless cable equation

$$x = X/\lambda \text{ and } g(x) = r_m G(x) \tag{49}$$

$$-\frac{\partial^2 V}{\partial x^2}+\frac{\partial V}{\partial t}+V=g(x,t)(E-V). \tag{50}$$

For steady-state solutions obtained with $\partial V/\partial t = 0$ and $g(x, t) = g(x)$, (50) reduces to (12).

## Appendix C: Steady-State Solution of the Cable Equation for Uniform Stimulation of the Sensory Dendrite

We consider the case in which the proximal part of the cable (up to $x_1$, corresponding to the sensory dendrite) is uniformily stimulated, $g(x) = \bar{g}$, and the rest of the cable (from $x_1$ to infinity) is purely passive, $g(x) = 0$. The steady-state receptor potential $V = V(x)$ satisfies the differential Eq. (12). We solve this equation by imposing the two boundary conditions, $V(\infty)$ bounded and $V'(0) = 0$ ('sealed end'). Equation (12) will be solved in regions $0 \le x < x_1$ and $x \ge x_1$ separately. Then the solutions will be connected to achieve continuity of the potential and longitudinal current,

$$\begin{aligned} V(x_1^-) &= V(x_1^+) \\ V'(x_1^-) &= V'(x_1^+). \end{aligned} \tag{51}$$

To get the complete solution of (12), we need to solve the homogeneous counterpart of (12). For $0 \le x < x_1$ it can be written in the form

$$-\frac{\mathrm{d}^2 V}{\mathrm{d}x}+(1+\bar{g})V=0 \tag{52}$$

with solution

$$V_h = c_1\exp\left(-\sqrt{1+\bar{g}}x\right)+c_2\exp\left(\sqrt{1+\bar{g}}x\right). \tag{53}$$

The complete solution of (12) can be written in the form

$$\begin{aligned} V(x) = {} & c_1\exp\left(-\sqrt{1+\bar{g}}x\right) \\ & +c_2\exp\left(\sqrt{1+\bar{g}}x\right)+\frac{E\bar{g}}{1+\bar{g}}. \end{aligned} \tag{54}$$

For $x \ge x_1$, where $\bar{g} = 0$, we have

$$V(x) = d_1\exp(-x)+d_2\exp(x). \tag{55}$$

The constants $c_1$, $c_2$, $d_1$, and $d_2$ must be determined from the boundary conditions. The condition of boundedness at $x = \infty$ implies $d_2 = 0$. Imposing the continuity conditions (51) we obtain

$$\begin{aligned} & c_1\exp\left(-\sqrt{1+\bar{g}}x\right)+c_2\exp\left(\sqrt{1+\bar{g}}x\right) \\ & +\frac{E\bar{g}}{1+\bar{g}} = d_1\exp(-x_1), \end{aligned} \tag{56}$$

and

$$\begin{aligned} & -c_1\sqrt{1+\bar{g}}\exp\left(-\sqrt{1+\bar{g}}x\right)+c_2\sqrt{1+\bar{g}} \\ & \times\exp\left(\sqrt{1+\bar{g}}x\right) = -d_1\exp(-x_1). \end{aligned} \tag{57}$$

The condition of zero longitudinal current $V'(0) = 0$ at $x = 0$ applied to (54) gives $c_1 = c_2$ and combining

(56) and (57) we obtain

$$c_1 = \frac{E\bar{g}}{1+\bar{g}} \times \left\{ \frac{1}{\left(\sqrt{1+\bar{g}}-1\right)\exp\left(-\sqrt{1+\bar{g}}x_1\right) - \left(\sqrt{1+\bar{g}}+1\right)\exp\left(\sqrt{1+\bar{g}}x_1\right)} \right\} \tag{58}$$

and

$$d_1 = \frac{E\bar{g}}{1+\bar{g}}\exp(x_1) \times \left\{ \frac{2\cosh(\sqrt{1+\bar{g}}x_1)}{\left(\sqrt{1+\bar{g}}-1\right)\exp\left(-\sqrt{1+\bar{g}}x_1\right) - \left(\sqrt{1+\bar{g}}+1\right)\exp\left(\sqrt{1+\bar{g}}x_1\right)} + 1 \right\} \tag{59}$$

Thus, for $0 \leq x \leq x_1$ we get (14) and for $x \geq x_1$, (15).

## Acknowledgments

We wish to thank Prof. K.-E. Kaissling and Dr. John Thorson for helpful discussions in the course of this work. This research was partly supported by grant #309/95/0627 from the Grant Agency of the Czech Republic and a fellowship from the Institut National de la Recherche Agronomique (to P.L.).

## References

Av-Ron E (1994) The role of a transient potassium current in a bursting neuron model. *J. Math. Biol.* 33:71–87.

Boekhoff I, Seifert E, Göggerle S, Lindemann M, Krüger B-W, Breer H (1993) Pheromone-induced second-messenger signaling in insect antennae. *Insect Biochem. Molec. Biol.* 23:757–762.

Breer H (1994) Odor recognition and second messenger signaling in olfactory receptor neurons. *Seminars in Cell Biol.* 5:25–32.

Breer H, Boekhoff I, Tareilus E (1990) Rapid kinetics of second messenger formation in olfactory transduction. *Nature* 345: 65–68.

Bressloff, PC (1995) Dynamics of a compartmental model integrate-and-fire neuron with somatic potential reset. *Physica D* 80:399–412.

De Kramer JJ (1985) The electrical circuitry of an olfactory sensillum in *Antheraea polyphemus*. *J. Neurosci.* 5:2484–2493.

De Kramer JJ, Kaissling K-E, Keil T (1984) Passive electrical properties of insect olfactory sensilla may produce the biphasic shape of spikes. *Chem. Senses* 8:289–295.

Duchamp-Viret P, Duchamp A, Vigouroux M (1989) Amplifying role of convergence in olfactory system: a comparative study of receptor cell and second order neuron sensitivities. *J. Neurophysiol.* 61:1085–1094.

Ennis DM (1991) Molecular mixture models based on competitive and non-competitive agonism. *Chem. Senses* 16:1–17.

Firestein S (1992) Electrical signals in olfactory transduction. *Current Opinion Neurobiol.* 2:444–448.

Gerstner W, van Hemmen JL (1992) Universality in neural networks: The importance of the 'mean firing rate'. *Biol. Cybern.* 67:195–205.

Getchell TV, Shepherd GM (1978) Responses of olfactory receptor cells to step pulses of odour at different concentrations in the salamander. *J. Physiol. Lond.* 282:521–540

Getz WM, Akers RP (1995) Partitioning non-linearities in the response of honey bee olfactory receptor neurons to binary odors. *BioSystems* 34:27–40.

Hahn I, Scherer PW, Mozell MM (1994) A mass transport model of olfaction. *J. Theor. Biol.* 167:115–128.

Kaissling K-E (1969) Kinetics of olfactory receptor potentials. In: C Pfaffman, ed. Olfaction and Taste III. Rockfeller University Press, New York. pp. 52–70.

Kaissling K-E (1971) Insect olfaction. In: LM Beidler, ed. Handbook of sensory physiology. Springer-Verlag, Berlin. pp. 351–431.

Kaissling K-E (1977) Structures of odour molecules and multiple activities of receptor cells. In: J Le Magnen, P MacLeod, eds. Olfaction and Taste VI. IRL, London. pp. 9–16.

Kaissling K-E (1986) Chemo-electrical transduction in insect olfactory receptors. *Ann. Rev. Neurosci.* 9:121–145.

Kaissling K-E (1987) R.H. Wright lectures on insect olfaction. In: K Colbow, ed. Simon Fraser University, Canada.

Kaissling K-E (1990) Antennae and noses: their sensitivities as molecule detectors. In: Borsellino et al., eds. Sensory transduction. Plenum, New York. pp. 81–97.

Kaissling K-E (1994) Elementary receptor potentials of insect olfactory cells. In: K Kurihara, N Suzuki, H Ogawa, eds. Olfaction and Taste XI, Springer Verlag, Tokyo. pp. 812–815.

Kaissling K-E, Boeckoff I (1993) Transduction and intracellular messengers in pheromone receptor cell of the moth *Antheraea polyphemus*. In: K Wiese, FG Gribakin, AV Popov, G Renninger, eds. Sensory systems of arthropods. Birkhä user Verlag, Basel. pp. 489–502.

Kaissling K-E, Priesner E (1970) Die Riechschwelle des Seidenspinners. *Naturwissenschaften* 57:23–28.

Kaissling K-E, Thornson J (1980) Insect olfactory sensilla: Structural, chemical and electrical aspects of the functional organization. In: DB Sattelle, LM Hall, JG Hildebrand, eds. Receptors for neurotransmitters, hormones and pheromones in insects. Elsevier/North-Holland, Amsterdam. pp. 261–282.

Keil T (1984) Reconstruction and morphometry of silkmoth olfactory hairs: A comparative study of sensilla trichodea on the antennae of male *Antheraea polyphemus* and *Antheraea pernyi* (Insecta, Lepidoptera). *Zoomorphology* 104:147–156.

Lamb TD, Pugh EN (1992) G-protein cascades: Gain and kinetics. *Trends in Neurosci.* 15:291–298.

Lánský P, Rospars J-P (1993) Coding of odor intensity. *BioSystems* 31:15–38.

Lánský P, Rospars J-P (1995) Ornstein-Uhlenbeck neuron revisited. *Biol. Cybern.* 72:397–406.

Lánský P, Rospars J-P, Vermeulen A (1994) Basic mechanisms of coding stimulus intensity in the olfactory sensory neuron. *Neural Processing Letters* 1:9–13.

Lowe G, Gold GH (1995) Olfactory transduction is intrinsically noisy. *Proc. Natl. Acad. Sci.* 92:7864–7868.

Lundström KI, Karlsson JOG, Svensson SPS, Mårtensson LGE, Elwing H, Ödman S, Andersson RGG (1993) Local and non-local receptor signalling. *J. Theor. Biol.* 164:135–148.

Lynch JW, Barry PH (1989) Action potentials initiated by single channels opening in a small neuron (rat olfactory receptor). *Biophys. J.* 55:755–768.

Malaka R, Ragg T, Hammer M (1995) A model of chemosensory reception. In: G Tesawo, D Touretzky, J Alspector, eds. Advances in neural information processing systems, Vol. 7, Morgan Kaufmann, San Mateo.

Menini A, Picco C, Firestein S (1995) Quantal-like current fluctuations induced by odorants in olfactory receptor cells. *Nature* 373:435–437.

Nicolis G, Prigogine I (1977) Selforganization in nonequilibrium systems. Wiley, New York.

O'Connel RJ, Mozell MM (1969) Quantitative stimulation of frog olfactory receptors. *J. Neurophysiol.* 32:51–63.

Pongracz F, Firestein S, Shepherd GM (1991) Electrotonic structure of olfactory sensory neurons analyzed by intracellular and whole cell patch techniques. *J. Neurophysiol.* 65:747–758.

Rall W (1977) Core conductor theory and cable properties of neurons. In: ER Kandel, JM Brookhardt, VB Mountcastle, eds. Handbook of physiology: The nervous system, Vol. 1. Williams and Wilkins, Baltimore. pp. 39–98.

Rall W (1989) Cable theory for dendritic neurons. In: C Koch, I Segev, eds. Methods in neuronal modeling. MIT Press, Cambridge. pp. 9–62.

Rospars J-P, Lánský P (1993) Stochastic model neuron without resetting of dendritic potential: application to the olfactory system. *Biol. Cyb.* 69:283–294.

Rospars J-P, Lánský P, Vaillant J, Duchamp-Viret P, Duchamp A (1994) Spontaneous activity of first- and second-order neurons in the frog olfactory system. *Brain Res.* 662:31–44.

Rovinsky A, Menzinger M (1993) Dynamics of analog-to-frequency transduction by excitable systems: Sensory receptors. *J. Chem. Phys.* 98:9155–9166.

Schwaber JS, Graves EB, Paton JFR (1993) Computational modeling of neuronal dynamics for systems analysis: application to neurons of the cardiorespiratory NTS in the rat. *Brain Res.* 604: 126–141.

Segev I (1992) Single neurone models: oversimple, complex and reduced. *Trends in Neurosci.* 15:414–421.

Segundo JP, Vibert J-F, Pakdaman K, Stiber M, Diez Martínez O (1994) Noise and the neurosciences: a long history, a recent revival and some theory. In: K Pribram, ed. Origins: brain and self-organization. Lawrence Erlbaum, Hillsdale, NJ, pp. 300–331.

Selzer R (1984) On the specificities of antennal olfactory receptor cells of *Periplaneta americana*. *Chem. Senses* 8:375–395.

Shepherd GM (1994) Discrimination of molecular signals by the olfactory receptor neuron. *Neuron* 13:771–790.

Shirsat N, Siddiqi O (1993) Olfaction in invertebrates. *Current Opinion Neurobiol.* 3:553–557.

Stengl M, Hatt H, Breer H (1992) Peripheral processes in insect olfaction. *Ann. Rev. Physiol.* 54:665–681.

Tateda H (1967) Sugar receptor and $\alpha$-amino acid in the rat. In: T Hayashi, ed. Olfaction and Taste II, Pergamon Press. pp. 383–397.

Tuckwell HC (1988) Introduction to theoretical Neurobiology. Cambridge University Press, New York.

Tuckwell HC, Rospars J-P, Vermeulen A, Lánský P (1995) Time-dependent solutions for a cable model of an olfactory receptor neuron. Submitted.

Vareschi E (1971) Duftunterscheidung bei der Honigbiene. Einzelzell-Ableitungen und Verhaltensreaktionen. *Z. Vergl. Physiol.* 75:143–173.

Vermeulen A, Rospars J-P, Lánský P, Tuckwell HC (1995) Coding of stimulus intensity in an olfactory receptor neuron: role of neuron spatial extension and dendritic backpropagation of action potentials. *Bull. Math. Biol.* In press.

Wilson MA, Bower JM (1989) The simulation of large-scale neural networks. In: C Koch, I Segev, eds. Methods in neuronal modeling. MIT Press, Cambridge, MA. pp. 291–333.

Yamada WM, Koch C, Adams PR (1989) Multiple channels and calcium dynamics. In: C Koch, I Segev, eds. Methods in neuronal modeling. MIT Press, Cambridge, MA. pp. 97–133.

Yu X, Lewis ER (1989) Studies with spike initiators: linearizations by noise allows continuous signal modulation in neural networks. *IEEE Trans. Biomed. Eng.* 36:36–43.

Zufall F, Stengl M, Franke C, Hildebrand JG, Hatt H (1991) Ionic currents of cultured olfactory receptor neurons from antennae of male *Manduca sexta*. *J. Neurosci.* 11:956–965.